Radiative corrections to $ZZ \rightarrow ZZ$ in the electroweak standard model

A. Denner

Paul Scherrer Institut, Würenlingen und Villigen, CH-5232 Villigen PSI, Switzerland

S. Dittmaier

Theoretische Physik, Universität Bielefeld, Postfach 100131, D-33501 Bielefeld, Germany

T. Hahn

Institut für Theoretische Physik, Universität Würzburg, Am Hubland, D-97074 Würzburg, Germany

(Received 19 December 1996)

The cross section for $ZZ \rightarrow ZZ$ with arbitrarily polarized Z bosons is calculated within the electroweak standard model including the complete $O(\alpha)$ corrections. We show the numerical importance of the radiative corrections and elaborate its characteristic features. The treatment of the Higgs-boson resonance is discussed in different schemes including the S-matrix-motivated pole scheme and the background-field method. The numerical accuracy of the equivalence theorem is investigated by comparing the cross sections for purely longitudinal Z bosons obtained from the equivalence theorem and from the complete calculation. In this context the full $O(\alpha)$ corrections are also confronted with the enhanced corrections of $O(\alpha M_H^2/s_W^2 M_W^2)$, which were frequently used in the literature. [S0556-2821(97)00513-4]

PACS number(s): 12.15.Lk, 11.15.Bt, 14.70.Hp

I. INTRODUCTION

Gauge-boson scattering provides a window into the heart of spontaneously broken gauge theories: the gauge-boson self-interactions and the scalar sector, which drives spontaneous symmetry breaking. Therefore, such processes found continuous interest in the literature [1–8] since the very first years of spontaneously broken gauge theories. Since lowest-order predictions for all gauge-boson scattering amplitudes involve only interactions between gauge and scalar bosons, the corresponding cross sections depend very sensitively on the non-Abelian and scalar sector of the underlying theory. This sensitivity is even enhanced for high-energetic, longitudinally polarized massive gauge bosons, due to the presence of gauge cancellations. A longitudinal polarization vector contains a factor k^0/M, where k^μ and M are the momentum and mass of the corresponding gauge boson, respectively, and induces contributions to the matrix element that grow with energy. In spontaneously broken gauge theories such contributions cancel in the high-energy limit, as required by unitarity. For 't Hooft gauge-fixing conditions these so-called unitarity cancellations are quantitatively expressed by the Goldstone-boson equivalence theorem (ET) [9–13] which relates amplitudes for longitudinal gauge bosons to those of the corresponding Goldstone bosons and thus reflects the connection between gauge and scalar sector of the theory.

In the minimal $SU(2) \times U(1)$ electroweak standard model (SM) only one physical scalar field remains after spontaneous symmetry breaking, viz., the Higgs boson, which plays a central role in the discussion of massive gauge-boson scattering. Virtual Higgs-boson exchange is needed to prevent the $2 \rightarrow 2$ scattering amplitudes of longitudinal gauge bosons from violating the (perturbative) unitarity bound at high energies. In turn, the requirement of unitarity can be used to derive bounds on the Higgs-boson mass below which the SM

remains weakly interacting and treatable in low-order perturbation theory [1,2]. These bounds are of the order of 1 TeV and are slightly strengthened by including the $O(\alpha M_H^2/s_W^2 M_W^2)$ radiative corrections (RC's) to gauge-boson scattering [4]. As already pointed out in Ref. [3], all these bounds are only qualitative, since they are obtained by applying perturbation theory in a region where it breaks down. The bounds on M_H can be related to a scale of new physics, which is necessary to avoid the Landau pole in the scalar self-interaction [5]. If these bounds are not satisfied the Higgs sector becomes strongly interacting. In this case large effects of new physics should arise in gauge-boson scattering and these processes would be particularly suited to study the electroweak symmetry breaking sector of the SM [2,10,14].

Gauge-boson scattering reactions can be studied at all high-energy colliders, i.e., pp colliders such as the CERN Large Hadron Collider (LHC), e^+e^- colliders such as the Next Linear Collider (NLC), or $\mu^+\mu^-$ colliders, where these reactions naturally appear as subprocesses. At high energies ($E \gg M_W$) the incoming particles radiate plenty of gauge bosons. Similar to the well-known Weizsäcker-Williams approximation for photonic reactions also massive vector-boson scattering at high energies can be approximated by convoluting the vector-boson cross section with the corresponding flux of gauge bosons. This approximation is known as equivalent vector-boson method (see, e.g., Ref. [15], and references therein).

At high energies, where the investigation of gauge-boson scattering is most interesting, the RC's are typically large and need to be taken into account. In this paper we investigate the effects of RC's on on-shell massive gauge-boson scattering processes. We have chosen the simplest representative, the process $ZZ \rightarrow ZZ$. It contains all interesting features that are typical for massive gauge-boson scattering such as the occurrence of a Higgs-boson resonance or enhanced

RC's associated with a heavy Higgs boson. On the other hand, complications by bremsstrahlung corrections, which occur for W bosons, are absent.

We calculate the complete $O(\alpha)$ RC's to $ZZ \rightarrow ZZ$ and present a detailed numerical discussion of the $O(\alpha)$-corrected cross sections both for the unpolarized case and the most interesting individual polarizations. Once RC's are taken into account, the introduction of a finite decay width of the Higgs boson, which is necessary for a sensible description of the resonance, is nontrivial owing to problems with gauge invariance. We compare different treatments such as the naive introduction of a finite width, Laurent expansions about the complex pole, as well as Dyson summations of self-energy corrections. The latter procedure is, in particular, applied within the framework of the background-field method (BFM) (see Ref. [16], and references therein), where Dyson summation does not disturb the underlying Ward identities [13] which guarantee gauge cancellations and unitarity.

For longitudinal gauge-boson scattering the radiative corrections of $O(\alpha M_H^2/s_W^2 M_W^2)$, which dominate for a heavy Higgs boson, have been calculated in the literature using the ET. We test the accuracy of such an approach by comparing these results with the full $O(\alpha)$ corrections. Moreover, we have calculated the $O(\alpha)$ corrections as predicted via the ET, which possess a very simple analytical form.

This paper is organized as follows. After some preliminary remarks in Sec. II about kinematics, conventions, and discrete symmetries, we discuss the lowest-order cross sections in Sec. III. In Sec. IV we describe the explicit calculation and the structure of the $O(\alpha)$ corrections. The different methods for introducing a finite Higgs-boson width are presented in Sec. V. A brief description of the application of the ET to $Z_L Z_L \rightarrow Z_L Z_L$ and the heavy-Higgs-boson effects in Sec. VI concludes our presentation of the calculational framework. Numerical results are discussed in Sec. VII, and Sec. VIII contains our conclusions. Appendix A provides a further discussion of the Landau singularity that appears in some box diagrams. In Appendix B we present the full analytical results for the $O(\alpha)$ corrections obtained via the ET.

II. PRELIMINARIES

A. Kinematics and conventions

We consider the reaction

$$Z(k_1,\lambda_1) + Z(k_2,\lambda_2) \rightarrow Z(k_3,\lambda_3) + Z(k_4,\lambda_4), \quad (1)$$

where k_i and λ_i denote the momenta and helicities of the incoming and outgoing Z bosons, respectively. We use the indices L, T, and U to indicate longitudinal ($\lambda = 0$), transverse ($\lambda = \pm$), and unpolarized Z bosons, respectively, and characterize definite polarization combinations by a sequence of four letters, e.g., $LTLT$ stands for $Z_L Z_T \rightarrow Z_L Z_T$.

The incoming particles travel along the z axis and are scattered into the x-z plane. In the center-of-mass system (c.m.s.) the momenta and polarization vectors $\varepsilon_i(\lambda_i)$ read

$$k_1^\mu = (E,0,0,-p), \quad k_3^\mu = (E,-p\,\sin\theta,0,-p\,\cos\theta),$$

$$\varepsilon_1^\mu(0) = (-p,0,0,E)/M_Z,$$

$$\varepsilon_3^{\mu,*}(0) = (p,-E\,\sin\theta,0,-E\,\cos\theta)/M_Z,$$

$$\varepsilon_1^\mu(\pm) = (0,-1,\pm i,0)/\sqrt{2},$$

$$\varepsilon_3^{\mu,*}(\pm) = (0,-\cos\theta,\mp i,\sin\theta)/\sqrt{2},$$

$$k_2^\mu = (E,0,0,p), \quad k_4^\mu = (E,p\,\sin\theta,0,p\,\cos\theta),$$

$$\varepsilon_2^\mu(0) = (-p,0,0,-E)/M_Z,$$

$$\varepsilon_4^{\mu,*}(0) = (p,E\,\sin\theta,0,E\,\cos\theta)/M_Z,$$

$$\varepsilon_2^\mu(\pm) = (0,1,\pm i,0)/\sqrt{2},$$

$$\varepsilon_4^{\mu,*}(\pm) = (0,\cos\theta,\mp i,-\sin\theta)/\sqrt{2}, \quad (2)$$

in terms of the energy E of the Z bosons, their momentum $p = \sqrt{E^2 - M_Z^2}$, and the scattering angle θ. The Mandelstam variables are defined as

$$s = (k_1 + k_2)^2 = 4E^2,$$

$$t = (k_1 - k_3)^2 = -4p^2\,\sin^2\theta/2,$$

$$u = (k_1 - k_4)^2 = -4p^2\,\cos^2\theta/2. \quad (3)$$

Following the treatment of Ref. [17] for $\gamma\gamma \rightarrow WW$, we introduce the 83 standard matrix elements (SME's) $\mathcal{M}_{ijkl}$ which contain the complete information about the boson polarizations.[1] The invariant matrix element $\mathcal{M}$ is decomposed into a linear combination of the SME's with invariant functions $F_{ijkl}(s,t)$ as coefficients. Exploiting discrete symmetries, the number of independent SME's can be reduced.

In terms of the invariant matrix element $\mathcal{M}$ the differential cross section is expressed as

$$\left(\frac{d\sigma}{d\Omega}\right)_{\lambda_1\lambda_2\lambda_3\lambda_4} = \frac{1}{64\pi^2 s}\,|\mathcal{M}_{\lambda_1\lambda_2\lambda_3\lambda_4}|^2. \quad (4)$$

The unpolarized cross section results from an average over the initial states and a sum over the final states:

$$\left(\frac{d\sigma}{d\Omega}\right)_{\text{unpol}} = \frac{1}{9}\sum_{\lambda_1,\lambda_2}\sum_{\lambda_3,\lambda_4}\left(\frac{d\sigma}{d\Omega}\right)_{\lambda_1\lambda_2\lambda_3\lambda_4}. \quad (5)$$

More generally, the correct average is obtained by multiplying with 1/3 for each unpolarized Z boson and by 1/2 for each transverse Z boson in the initial state.

The integrated cross section is obtained by

$$\sigma_{\text{tot}} = \frac{1}{2}\int_{0°}^{360°}d\varphi\int_{\theta_{\text{cut}}}^{180°-\theta_{\text{cut}}}d\theta\,\sin\theta\,\frac{d\sigma}{d\Omega}, \quad (6)$$

---

[1]Only 81 SME's are linearly independent, the other two are kept for convenience.

where θ_{cut} denotes an angular cut which is set to 10° in our numerical evaluations. The symmetry factor 1/2 results from the presence of two identical particles in the final state.

B. Discrete symmetries

As a consequence of Bose symmetry the amplitude $\mathcal{M}$ is invariant under the interchange $(k_1, \varepsilon_1) \leftrightarrow (k_2, \varepsilon_2)$ and/or $(k_3, \varepsilon_3^*) \leftrightarrow (k_4, \varepsilon_4^*)$: i.e.,

$$
\begin{aligned}
\mathcal{M}_{\lambda_1 \lambda_2 \lambda_3 \lambda_4}(E, \theta) &= \mathcal{M}_{\lambda_2 \lambda_1 \lambda_4 \lambda_3}(E, \theta) \\
&= \mathcal{M}_{\lambda_1 \lambda_2 \lambda_4 \lambda_3}(E, 180° + \theta) \\
&= \mathcal{M}_{\lambda_2 \lambda_1 \lambda_3 \lambda_4}(E, 180° + \theta).
\end{aligned} \quad (7)
$$

This implies, for the cross sections,

$$
\begin{aligned}
\left(\frac{d\sigma}{d\Omega} \right)_{\lambda_1 \lambda_2 \lambda_3 \lambda_4}(s,t) &= \left(\frac{d\sigma}{d\Omega} \right)_{\lambda_2 \lambda_1 \lambda_4 \lambda_3}(s,t) \\
&= \left(\frac{d\sigma}{d\Omega} \right)_{\lambda_2 \lambda_1 \lambda_3 \lambda_4}(s,u) \\
&= \left(\frac{d\sigma}{d\Omega} \right)_{\lambda_1 \lambda_2 \lambda_4 \lambda_3}(s,u).
\end{aligned} \quad (8)
$$

In particular, all cross sections with equally polarized incoming and/or outgoing Z bosons are forward-backward symmetric.

CPT symmetry entails

$$
\mathcal{M}_{\lambda_1 \lambda_2 \lambda_3 \lambda_4} = \mathcal{M}_{\lambda_3 \lambda_4 \lambda_1 \lambda_2} \quad (9)
$$

and the analogous relation for the cross sections.

Because quark mixing is completely negligible for this process, we use a unit quark-mixing matrix, and thus also CP is an exact symmetry.[2] As a consequence, the helicity amplitudes are related as follows:

$$
\mathcal{M}_{\lambda_1 \lambda_2 \lambda_3 \lambda_4} = \mathcal{M}_{-\lambda_1 -\lambda_2 -\lambda_3 -\lambda_4}, \quad (10)
$$

and the cross sections do not change if all helicities are reversed.

Owing to CP invariance all SME's involving the totally antisymmetric Levi-Civita tensor drop out, and only 43 SME's can appear. As a consequence of Bose and CPT symmetry only the sum of each SME and the ones obtained from the interchanges $(\varepsilon_1, k_1, \varepsilon_3^*, k_3) \leftrightarrow (\varepsilon_2, k_2, \varepsilon_4^*, k_4)$ and $(\varepsilon_1, k_1, \varepsilon_2, k_2) \leftrightarrow (\varepsilon_3^*, k_3, \varepsilon_4^*, k_4)$ occur. This leaves 19 SME's, among which 17 are independent.

III. LOWEST-ORDER CROSS SECTION

To lowest order, only the three diagrams in Fig. 1 contribute and yield the following amplitude:
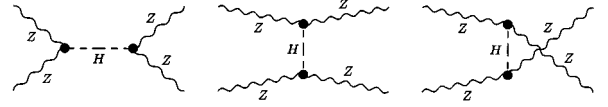
---

[2]Even for a general quark-mixing matrix, CP would be violated in the considered process only beyond the one-loop level.

FIG. 1. Lowest-order diagrams for $ZZ \to ZZ$.

$$
\mathcal{M}_{\mathrm{Born}} = -\frac{e^2 M_Z^2}{c_W^2 s_W^2} \left(\frac{\mathcal{M}_{00}^{(s)}}{s - M_H^2} + \frac{\mathcal{M}_{00}^{(t)}}{t - M_H^2} + \frac{\mathcal{M}_{00}^{(u)}}{u - M_H^2} \right), \quad (11)
$$

where $c_W = \cos \theta_W = M_W / M_Z$, $s_W = \sin \theta_W = \sqrt{1 - c_W^2}$, and the relevant SME's $\mathcal{M}_{00}^{(r)}$ are given by

$$
\mathcal{M}_{00}^{(s)} = (\varepsilon_1 \cdot \varepsilon_2)(\varepsilon_3^* \cdot \varepsilon_4^*), \quad \mathcal{M}_{00}^{(t)} = (\varepsilon_1 \cdot \varepsilon_3^*)(\varepsilon_2 \cdot \varepsilon_4^*),
$$

$$
\mathcal{M}_{00}^{(u)} = (\varepsilon_1 \cdot \varepsilon_4^*)(\varepsilon_2 \cdot \varepsilon_3^*). \quad (12)
$$

Explicit formulas for $\mathcal{M}_{\mathrm{Born}}$ for the 81 polarization combinations are listed in Table I. The dimensionful ZZH coupling leads to a suppression of the Born matrix element by a factor $M_Z^2 / |s - M_H^2|$ for $|s - M_H^2| \gg M_Z^2$. As a consequence, the lowest-order matrix element for purely transverse Z bosons is suppressed for high energies, $s \gg M_H^2$, by a factor M_Z^2 / s. Each longitudinal Z boson introduces a factor $\sqrt{s}/M_Z$ via its polarization vector. For helicity amplitudes with more than two external longitudinal Z bosons unitarity cancellations take place such that the Born matrix element with purely longitudinal Z bosons approaches a constant and those with three longitudinal Z bosons behave as $M_Z / \sqrt{s}$ at high energies. As a remnant of the unitarity cancellations the matrix elements involving four and three longitudinal Z bosons are enhanced by a factor M_H^2 / M_Z^2 if $M_Z^2 \ll M_H^2 \ll s$.

The analytical results for the asymptotic behavior of the integrated cross sections at high energies $(s \gg M_Z^2, M_H^2)$ are listed in Table II. The cross section for purely longitudinal Z bosons ($LLLL$) and the ones with two transverse and two longitudinal Z bosons ($LLTT, LTLT$) behave as $1/s$ for high energies. The cross sections with one or three longitudinal gauge bosons ($LTTT, LLLT$) are proportional to $1/s^2$, and the cross section for purely transverse Z bosons ($TTTT$) vanishes as $1/s^3$ at high energies for $\theta_{\mathrm{cut}} > 0$. When integrated over the full scattering angle the $TTTT$ cross section behaves as $1/s^2$ owing to the t- and u-channel poles. The cross sections not shown in Table II are obtained from the symmetry relations (8) and (9), e.g., $\sigma_{LLLT} = \sigma_{LLTL} = 2\sigma_{TLLL}$, where the factor 2 originates from the different spin average.

Figure 2 illustrates the (exactly calculated) polarized lowest-order cross sections integrated over $\theta_{\mathrm{cut}} < \theta < 180° - \theta_{\mathrm{cut}}$ for $\theta_{\mathrm{cut}} = 10°$ and a low Higgs-boson mass of $M_H = 100$ GeV. In Fig. 3 we show the same cross sections for $M_H = 700$ GeV using a naive constant finite width to describe the Higgs-boson resonance, as discussed in Sec. V below. The enhancement of the $LLLL$ and $LLLT$ cross sections caused by the factor M_H^2 / M_Z^2 can be seen by comparing Figs. 2 and 3. The Higgs-boson resonance occurs only for equally polarized Z bosons in the initial and final state, $\lambda_1 = \lambda_2$, $\lambda_3 = \lambda_4$. At lowest order, the $LLLL$ cross section dominates independently of the Higgs-boson mass.

TABLE I. Polarized lowest-order matrix elements ($\mathcal{S}=s-M_H^2$, $\mathcal{T}=t-M_H^2$, $\mathcal{U}=u-M_H^2$, and $\widetilde{s}=s-4M_Z^2$).

Polarization	$\mathcal{M}_{\text{Born}}=-\dfrac{e^2}{c_w^2 s_w^2}\times(\text{entry})$	Polarization	$\mathcal{M}_{\text{Born}}=-\dfrac{e^2}{c_w^2 s_w^2}\times(\text{entry})$
$LLLL$	$\dfrac{1}{4M_Z^2}\left[\dfrac{(s-2M_Z^2)^2}{\mathcal{S}}+\dfrac{[s(u-t)+\widetilde{s}^2]^2}{4\widetilde{s}^2\mathcal{T}}+\dfrac{[s(t-u)+\widetilde{s}^2]^2}{4\widetilde{s}^2\mathcal{U}}\right]$		
$\pm LLL$ $L\pm LL$ $LL\pm L$ $LLL\pm$	$\dfrac{1}{4\sqrt{2}M_Z}\dfrac{\sqrt{stu}}{\widetilde{s}^2}\left[\dfrac{s(u-t)+\widetilde{s}^2}{\mathcal{T}}-\dfrac{s(t-u)+\widetilde{s}^2}{\mathcal{U}}\right]$		
$LL\pm\pm$ $\pm\pm LL$	$\dfrac{s-2M_Z^2}{2\mathcal{S}}+\dfrac{stu}{2\widetilde{s}^2}\left[\dfrac{1}{\mathcal{T}}+\dfrac{1}{\mathcal{U}}\right]$	$LL\pm\mp$ $\pm\mp LL$	$\dfrac{stu}{2\widetilde{s}^2}\left[\dfrac{1}{\mathcal{T}}+\dfrac{1}{\mathcal{U}}\right]$
$\pm L\pm L$ $L\pm L\pm$	$\dfrac{u}{4\widetilde{s}^2}\left[-\dfrac{s(u-t)+\widetilde{s}^2}{\mathcal{T}}+\dfrac{2st}{\mathcal{U}}\right]$	$\pm L\mp L$ $L\pm L\mp$	$\dfrac{t}{4\widetilde{s}^2}\left[\dfrac{s(u-t)+\widetilde{s}^2}{\mathcal{T}}+\dfrac{2su}{\mathcal{U}}\right]$
$\pm LL\pm$ $L\pm\pm L$	$\dfrac{t}{4\widetilde{s}^2}\left[\dfrac{2su}{\mathcal{T}}-\dfrac{s(t-u)+\widetilde{s}^2}{\mathcal{U}}\right]$	$\pm LL\mp$ $L\pm\mp L$	$\dfrac{u}{4\widetilde{s}^2}\left[\dfrac{2st}{\mathcal{T}}+\dfrac{s(t-u)+\widetilde{s}^2}{\mathcal{U}}\right]$
$L\pm\pm\pm$ $\pm L\pm\pm$ $\pm\pm L\pm$ $\pm\pm\pm L$	$-\dfrac{M_Z}{\sqrt{2}}\dfrac{\sqrt{stu}}{\widetilde{s}^2}\left[\dfrac{u}{\mathcal{T}}-\dfrac{t}{\mathcal{U}}\right]$	$L\mp\pm\pm$ $\mp L\pm\pm$ $\pm\pm L\mp$ $\pm\pm\mp L$	$\dfrac{M_Z}{\sqrt{2}}\dfrac{\sqrt{stu}}{\widetilde{s}^2}\left[\dfrac{t}{\mathcal{T}}-\dfrac{u}{\mathcal{U}}\right]$
$L\pm\mp\pm$ $\pm L\pm\mp$ $\mp\pm L\pm$ $\pm\mp\pm L$	$-\dfrac{M_Z}{\sqrt{2}}\dfrac{u\sqrt{stu}}{\widetilde{s}^2}\left[\dfrac{1}{\mathcal{T}}+\dfrac{1}{\mathcal{U}}\right]$	$L\pm\pm\mp$ $\pm L\mp\pm$ $\pm\mp L\pm$ $\mp\pm\pm L$	$\dfrac{M_Z t\sqrt{stu}}{\sqrt{2}}\dfrac{}{\widetilde{s}^2}\left[\dfrac{1}{\mathcal{T}}+\dfrac{1}{\mathcal{U}}\right]$
$\pm\pm\pm\mp$ $\pm\pm\mp\pm$ $\pm\mp\pm\pm$ $\mp\pm\pm\pm$	$-M_Z^2\dfrac{tu}{\widetilde{s}^2}\left[\dfrac{1}{\mathcal{T}}+\dfrac{1}{\mathcal{U}}\right]$		
$\pm\mp\pm\mp$	$M_Z^2\dfrac{u^2}{\widetilde{s}^2}\left[\dfrac{1}{\mathcal{T}}+\dfrac{1}{\mathcal{U}}\right]$	$\pm\mp\mp\pm$	$M_Z^2\dfrac{t^2}{\widetilde{s}^2}\left[\dfrac{1}{\mathcal{T}}+\dfrac{1}{\mathcal{U}}\right]$
$\pm\pm\pm\pm$	$M_Z^2\left[\dfrac{1}{\mathcal{S}}+\dfrac{u^2}{\widetilde{s}^2\mathcal{T}}+\dfrac{t^2}{\widetilde{s}^2\mathcal{U}}\right]$	$\pm\pm\mp\mp$	$M_Z^2\left[\dfrac{1}{\mathcal{S}}+\dfrac{t^2}{\widetilde{s}^2\mathcal{T}}+\dfrac{u^2}{\widetilde{s}^2\mathcal{U}}\right]$

IV. RADIATIVE CORRECTIONS

A. Calculational framework

We have performed the calculation of the radiative corrections (RC's) in 't Hooft–Feynman gauge both in the conventional formalism and in the background-field formalism, applying the on-shell renormalization scheme in both cases. We follow the conventions of Ref. [18] for the conventional formalism and of Ref. [16] for the background-field formalism. In the conventional formalism the field renormalization is fixed such that no external wave-function renormalization is needed. In the renormalization scheme introduced in Ref. [16] for the background-field method the field renormalization is determined by gauge invariance, and a nontrivial external wave-function renormalization is required, as explicitly described in Ref. [13].

The Feynman graphs have been generated and drawn with FEYNARTS [19]. Both in the conventional formalism and in the background-field method we have performed two independent calculations.

One evaluation is based on the calculational method described in Ref. [18]. With the help of MATHEMATICA [20] the amplitudes are decomposed into SME's and invariant functions, and the one-loop contributions to the invariant functions are expressed in terms of standard tensor integrals. The tensor integrals are reduced to the standard scalar one-loop integrals, as described in Ref. [21]. The scalar one-loop integrals are evaluated using the methods and general results of Ref. [22]. The last two steps are performed numerically using own FORTRAN routines.

In the other calculation the algebra is performed with MATHEMATICA and FORM [23] and has been partially checked with FEYNCALC [24]. The resulting symbolic amplitudes are automatically converted into a FORTRAN program. Instead of using SME's, all scalar products of four-vectors are grouped together and calculated at run time by inserting

TABLE II. Polarized lowest-order cross sections at high energies ($s \gg M_Z^2, M_H^2$) integrated over $\theta_{\text{cut}} < \theta < 180° - \theta_{\text{cut}}$.

$$\sigma_{\text{Born}} = 2\pi \frac{1}{64\pi^2 s} \frac{e^4}{c_W^4 s_W^4} \times (\text{entry})$$

Polarization				
$LLLL$	$\dfrac{9M_H^4}{16M_Z^4} \cos\theta_{\text{cut}}$	$LLTT$ $\quad \dfrac{\cos\theta_{\text{cut}}}{2}$	$LTLT$ $\quad \dfrac{\cos\theta_{\text{cut}}}{4}$	
$LLLT$		$\dfrac{(M_H^2 + 2M_Z^2)^2}{2M_Z^2 s} \left\{ \ln \dfrac{s(1+\cos\theta_{\text{cut}})}{2M_H^2 + s(1-\cos\theta_{\text{cut}})} - \dfrac{2\cos\theta_{\text{cut}}(6M_H^2 + s\,\sin^2\theta_{\text{cut}})}{4M_H^2 + s\,\sin^2\theta_{\text{cut}}} \right\}$		
$LTTT$		$\dfrac{M_Z^2}{s} \left\{ 2\ln \dfrac{s(1+\cos\theta_{\text{cut}})}{2M_H^2 + s(1-\cos\theta_{\text{cut}})} - \dfrac{\cos\theta_{\text{cut}}(20M_H^2 + 3s\,\sin^2\theta_{\text{cut}})}{4M_H^2 + s\,\sin^2\theta_{\text{cut}}} \right\}$		
$TTTT$		$\dfrac{M_Z^4}{s^2} \left\{ -8\ln \dfrac{s(1+\cos\theta_{\text{cut}})}{2M_H^2 + s(1-\cos\theta_{\text{cut}})} + \dfrac{\cos\theta_{\text{cut}} s(8 + 11\sin^2\theta_{\text{cut}})}{4M_H^2 + s\,\sin^2\theta_{\text{cut}}} \right\}$		

the explicit representations (2) for the polarization vectors. The tensor integrals are numerically reduced to scalar integrals, which are evaluated using the FF package [25]. The code thus obtained executes favorably fast and numerically stable.

Because of the length of the results we do not list the analytical expressions but give only an inventory of the $O(\alpha)$ RC's and discuss some important features.

B. Inventory of $O(\alpha)$ corrections

Both in the conventional formalism and in the background-field formalism about 550 Feynman diagrams contribute to $ZZ \rightarrow ZZ$ at one-loop order. The one-loop corrections can be classified into self-energy corrections, vertex corrections, box corrections, and wave-function-renormalization corrections. All of them can be divided into s-, t-, and u-channel contributions, which are related by simple transformations. In the following we list only the s-channel Feynman graphs for the conventional formalism in 't Hooft–Feynman gauge.

The diagrams contributing to the self-energy corrections in the s channel are shown in Fig. 4. The diagram with a virtual W and ϕ field actually represents two diagrams with opposite charge flow. After renormalization the diagrams of Fig. 4 yield together with the corresponding t- and u-channel diagrams the following contribution to the invariant matrix element:
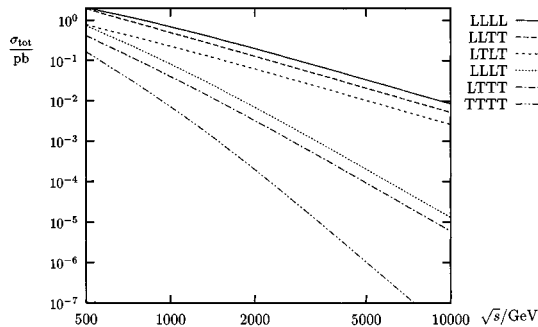
$$\delta\mathcal{M}_{\text{self}} = \frac{e^2 M_Z^2}{c_W^2 s_W^2} \left(\frac{\mathcal{M}_{00}^{(s)}}{(s - M_H^2)^2} \Sigma^H(s) + \frac{\mathcal{M}_{00}^{(t)}}{(t - M_H^2)^2} \Sigma^H(t) \right.$$
$$\left. + \frac{\mathcal{M}_{00}^{(u)}}{(u - M_H^2)^2} \Sigma^H(u) \right), \tag{13}$$

where Σ^H is the renormalized Higgs-boson self-energy.

For each of the six vertices appearing in the Born diagrams (Fig. 1) there is a set of vertex corrections. In Fig. 5 we show the diagrams that constitute the corrections to the final-state vertex in the s-channel diagram of Fig. 1. Note that each graph with three charged fields or two different charged fields in the loop represents two diagrams with opposite orientation of the charge flow. Owing to the simple tensor structure of the ZZH vertex, the vertex corrections have the relatively simple form

$$\delta\mathcal{M}_{\text{vertex}} = -\frac{e^2 M_Z^2}{c_W^2 s_W^2} \sum_{r=s,t,u} \frac{1}{r - M_H^2} [2\mathcal{M}_{00}^{(r)} F_0^{ZZH}(r)$$
$$+ (\mathcal{M}_{10}^{(r)} + \mathcal{M}_{01}^{(r)}) F_1^{ZZH}(r)] \tag{14}$$

with the two renormalized form factors $F_0^{ZZH}(r)$ and $F_1^{ZZH}(r)$ for each channel, the corresponding SME's $\mathcal{M}_{00}^{(r)}$ from Eq. (12), and

FIG. 2. Integrated lowest-order cross sections for various polarizations at $M_H = 100$ GeV.
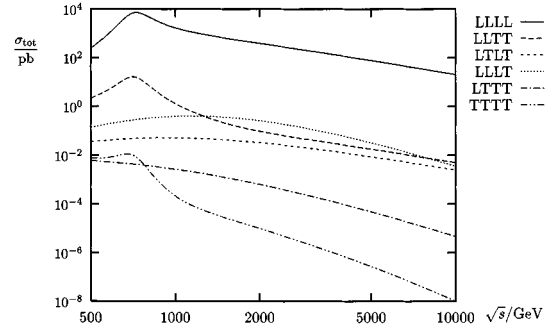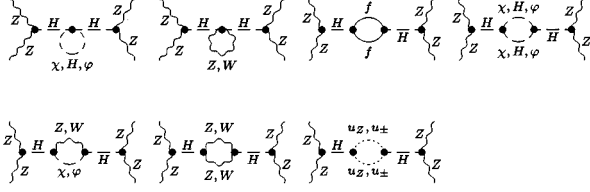

FIG. 3. Integrated lowest-order cross sections for various polarizations at $M_H = 700$ GeV.

FIG. 4. s-channel self-energy diagrams.

$$\mathcal{M}_{01}^{(s)} = (\varepsilon_1 \cdot \varepsilon_2)(\varepsilon_3^* \cdot k_4)(\varepsilon_4^* \cdot k_3)/s,$$

$$\mathcal{M}_{10}^{(s)} = (\varepsilon_3^* \cdot \varepsilon_4^*)(\varepsilon_1 \cdot k_2)(\varepsilon_2 \cdot k_1)/s,$$

$$\mathcal{M}_{01}^{(t)} = (\varepsilon_1 \cdot \varepsilon_3^*)(\varepsilon_2 \cdot k_4)(\varepsilon_4^* \cdot k_2)/s,$$

$$\mathcal{M}_{10}^{(t)} = (\varepsilon_2 \cdot \varepsilon_4^*)(\varepsilon_1 \cdot k_3)(\varepsilon_3^* \cdot k_1)/s,$$

$$\mathcal{M}_{01}^{(u)} = (\varepsilon_1 \cdot \varepsilon_4^*)(\varepsilon_2 \cdot k_3)(\varepsilon_3^* \cdot k_2)/s,$$

$$\mathcal{M}_{10}^{(u)} = (\varepsilon_2 \cdot \varepsilon_3^*)(\varepsilon_1 \cdot k_4)(\varepsilon_4^* \cdot k_1)/s. \tag{15}$$

The factors $1/s$ in Eq. (15) have been introduced to render the matrix elements dimensionless.

The s-channel box diagrams (i.e., those with natural variables s and t) are shown in Fig. 6. Note that again all graphs with three or four charged fields in the loop represent two Feynman diagrams with opposite orientation of the charge flow. The analytical expressions for the box diagrams are rather involved and require all CP-conserving SME's. It turns out that the results for the bosonic box diagrams are shorter by a factor of about 3/2 in the background-field formalism as compared to the conventional formalism. Because of the involved structure of the fermion-Z-boson couplings, the most complicated expressions are those for the fermionic box diagrams, which are identical in both formalisms.

Following the complete on-shell renormalization scheme of Ref. [18] for the conventional formalism the field renormalization is chosen such that no extra wave-function renormalization is necessary. However, in the on-shell renormalization scheme of Ref. [16] for the background-field formalism a nonvanishing wave-function renormalization for
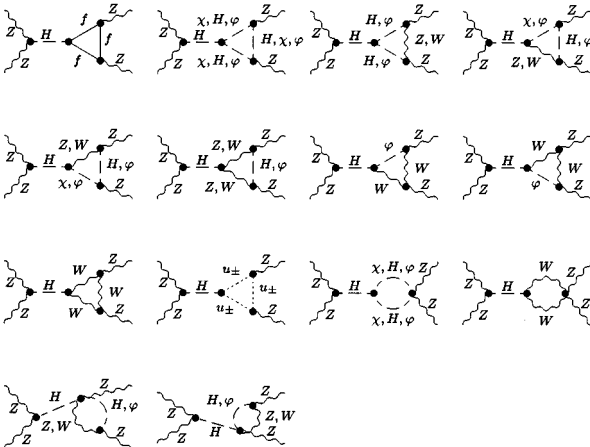
FIG. 5. s-channel final-state vertex diagrams.
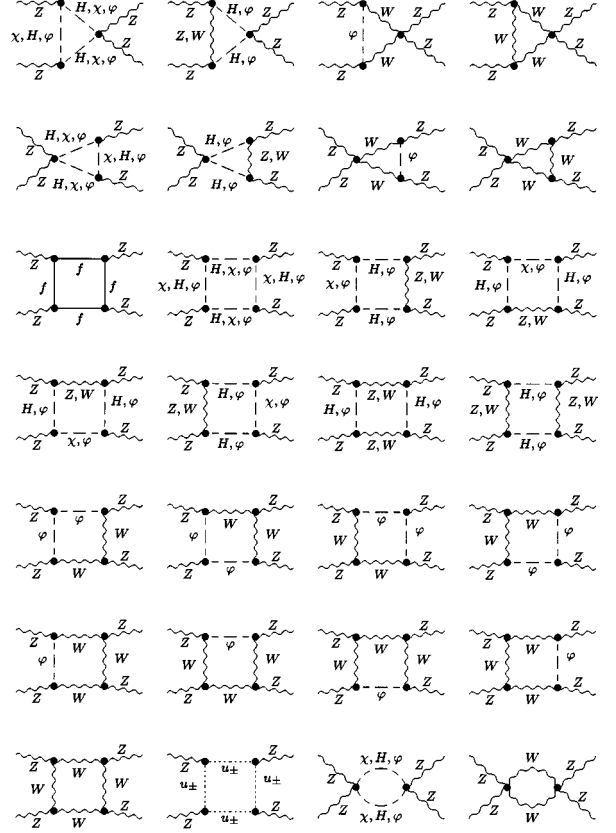
FIG. 6. s-channel box diagrams.

external particles is required. In a strict $O(\alpha)$ calculation the wave-function renormalization corrections are given by

$$\delta\mathcal{M}_{\mathrm{wf}} = 2\,\delta R_Z \mathcal{M}_{\mathrm{Born}}, \tag{16}$$

where

$$\delta R_Z = -\operatorname{Re}\{\Sigma_T'^{ZZ}(M_Z^2)\} \tag{17}$$

is the $O(\alpha)$ contribution to the wave-function renormalization constant $R_Z = 1 + \delta R_Z$. The function $\Sigma_T'^{ZZ}(s) = d\Sigma_T^{ZZ}(s)/ds$ denotes the derivative of the transverse part of the renormalized Z-boson self-energy.

Thus, the full one-loop matrix element reads

$$\delta\mathcal{M}_{\mathrm{one\ loop}} = \delta\mathcal{M}_{\mathrm{self}} + \delta\mathcal{M}_{\mathrm{vertex}} + \delta\mathcal{M}_{\mathrm{box}} + \delta\mathcal{M}_{\mathrm{wf}}. \tag{18}$$

C. Corrected cross section

It turns out that the $O(\alpha)$ corrections are comparable or even larger than the lowest-order contributions for various important configurations. In order to obtain meaningful predictions, it is therefore necessary to consider not only the interference between the lowest-order and the one-loop matrix element but to take into account the complete square of the matrix element and to define the corrected cross section as

$$\frac{d\sigma}{d\Omega} = \frac{1}{64\pi^2 s}\,|\mathcal{M}_{\mathrm{Born}} + \delta\mathcal{M}_{\mathrm{one\ loop}}|^2 \tag{19}$$

including the terms involving $|\delta\mathcal{M}_{\mathrm{one\ loop}}|^2$.

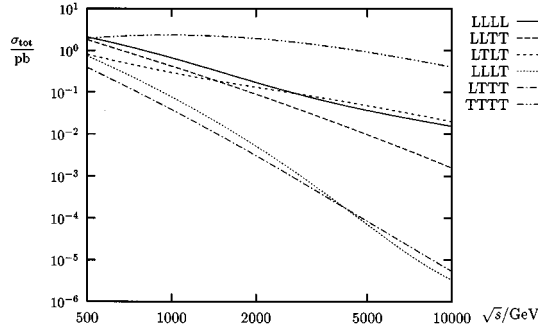FIG. 7. Integrated corrected cross sections for various polarizations at $M_H = 100$ GeV.

FIG. 8. Integrated corrected cross sections for various polarizations at $M_H = 700$ GeV.

In this way we end up with $O(\alpha)$ accuracy where $\mathcal{M}_{\mathrm{Born}}$ dominates and $O(1)$ accuracy otherwise (relative to the leading loop order). To obtain $O(\alpha)$ accuracy everywhere the $O(\alpha^2)$ corrections would be required. Note that the interference between $\delta \mathcal{M}_{2\ \mathrm{loop}}$ and $\mathcal{M}_{\mathrm{Born}}$ is suppressed with respect to $|\delta \mathcal{M}_{\mathrm{one\ loop}}|^2$ if the importance of $\delta \mathcal{M}_{\mathrm{one\ loop}}$ results from a suppression of $\mathcal{M}_{\mathrm{Born}}$ and not from the presence of an effective large loop-expansion parameter.

In Figs. 7 and 8 we show the corrected polarized cross sections as defined in Eq. (19). The Higgs-boson resonance in Fig. 8 is treated by Dyson summation within the BFM [cf. Section V B, Eq. (36)]. In the case of purely transverse Z bosons ($TTTT$) the cross section is drastically enhanced compared to the lowest order and behaves as $1/s$ at high energies (without cutoff it even would not go down with energy). For a small Higgs-boson mass this cross section becomes the dominating one. Apart from the $LTTT$ case, the corrections reach the size of the lowest-order cross sections for all polarizations. This is probably due to corrections of the form[3] $(\alpha/\pi)[\ln(s/M_Z^2)]^2 \approx 0.2$ that are further enhanced by numerical factors and t- and u-channel poles. The relative corrections depend only weakly on the Higgs-boson mass apart from the polarizations $LLLL$ and $LLLT$, where the corrections involve extra factors M_H/M_Z. As a consequence the $LLLL$ cross section dominates for a large Higgs-boson mass. As for the lowest-order cross sections, the Higgs-boson resonance only contributes for $\lambda_1 = \lambda_2$ and $\lambda_3 = \lambda_4$. For the $TTTT$ channel the resonance is proportional to the corresponding strongly suppressed Born cross section and thus not visible. Because the lowest-order cross sections are not dominating, the universal corrections associated with the running of α and the ρ parameter, which are related to the lowest order, are not leading.

D. Landau singularities in four-point functions

The four-point function [22]

$$D_0(M_Z^2, M_Z^2, M_Z^2, M_Z^2, t, u, m^2, m^2, m^2, m^2), \qquad (20)$$

exhibits a Landau singularity [27] of the form

---

[3] At high energies vertex and box corrections typically yield contributions of this kind, as, e.g., explicitly calculated for $e^+e^- \rightarrow W^+W^-$ in Ref. [26].
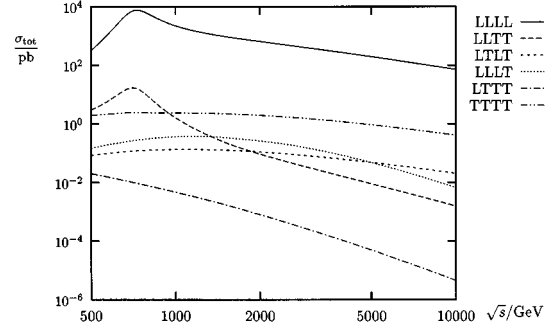
$$D_0 = D_0^{\mathrm{reg}} - \frac{\pi^2}{\sqrt{\Delta - i\varepsilon}} \qquad (21)$$

for $t < 0$, $u < 0$, and $M_Z > 2m$, where D_0^{reg} is regular and

$$\Delta = \frac{tu}{16}[(t - 4m^2)(u - 4m^2) - (2M_Z^2 - 4m^2)^2]. \qquad (22)$$

With $b = M_Z^4 - m^2 s$ and $p^2 = E^2 - M_Z^2$ this becomes

$$\Delta = (p^4 \sin^2\theta - b)p^4 \sin^2\theta. \qquad (23)$$

Squaring the matrix element promotes the root singularity at $p^2 \sin\theta = \pm\sqrt{b}$ to a pole which is not integrable and thus leads to a formally divergent cross section.

This singularity should disappear from physical observables. The condition $M_Z > 2m$ suggests that it is related to the instability of the Z bosons. In fact, as illustrated in Appendix A, it is canceled by diagrams that contribute to the inclusive process $ZZ \rightarrow 4f$, which cannot be separated from $ZZ \rightarrow ZZ$ once the decay of the Z bosons is taken into account. Moreover, one should notice that colliding Z bosons which are radiated off from incoming particles possess an invariant mass $q^2 < 0$ so that the condition $q^2 > 4m^2$ is never fulfilled in the physical region of phase space. The use of on-shell Z bosons ($q^2 = M_Z^2$) is just part of the equivalent vector-boson approximation.

The Landau singularity appears in practice for box diagrams involving light fermions, i.e., with $m = m_f \ll M_Z$. The location of the singularity in phase space for $m = 0$ is shown in Fig. 9. It appears at $\theta = 90°$ for $p^2 = M_Z^2$, i.e., $\sqrt{s} = 2\sqrt{2}M_Z \approx 258$ GeV, and moves fast towards the forward and backward directions with increasing energy. Its effect is most prominent at low energies and becomes small at high energies. Moreover, it is located outside the angular region $10° < \theta < 170°$ for $\sqrt{s} \gtrsim 500$ GeV for all fermions. In the following we always consider the cross section in regions where this singularity is absent or negligible.

V. HIGGS-BOSON RESONANCE

Diagrams that involve a Higgs-boson propagator in the s channel have a pole at $s = M_H^2$. The double pole in the self-energy diagrams of Fig. 4 is reduced to a single pole after Dyson summation.

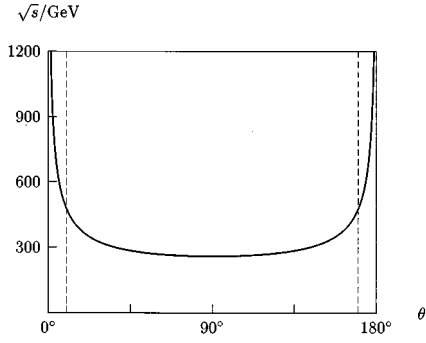If $M_H > 2M_Z$ a proper treatment of the resonance is nec-

FIG. 9. The location of the Landau singularities in the D_0 function (20) for $m=0$. The dashed lines at $\theta_{cut}=10°$ and $180°-\theta_{cut}=170°$ indicate the integration interval.

essary to render the cross section finite and meaningful. The naive introduction of a finite Higgs-boson width via the substitution

$$\frac{1}{s-M_H^2} \to \frac{1}{s-M_H^2+iM_H\Gamma_H} \qquad (24)$$

or naive Dyson summation

$$\frac{1}{s-M_H^2} \to \frac{1}{s-M_H^2+\Sigma^H(s)} \qquad (25)$$

amounts to an inclusion of an incomplete set of higher-order corrections such that the resulting matrix element becomes gauge dependent and does not respect the gauge cancellations, which guarantee a decent high-energy behavior necessary for unitarity.

It is perhaps useful to explain the last point in more detail. The validity of Ward identities is crucial to guarantee the unitarity of the S matrix in gauge theories. While the Ward identities relate Green functions, they nevertheless have a direct impact on physical amplitudes. Since the longitudinal

polarization vector of a massive gauge boson (with mass M and momentum k) behaves like k^μ/M at high energies, in the absence of gauge invariance, amplitudes involving longitudinal gauge bosons usually grow with energy and violate the unitarity bounds. In gauge theories, the Ward identities imply the Goldstone-boson equivalence theorem (ET) which ensures that the amplitudes involving longitudinal gauge bosons are well behaved at high energies. A violation of the relevant Ward identities, even by higher-order terms, leads to a violation of the ET and thus to amplitudes that violate unitarity. For the process $ZZ\to ZZ$ the unitarity-violating effects involve factors E/M_Z and overcome any constant suppression at sufficiently high energies.

A. Pole expansion

Since the poles of the S matrix are gauge independent, it has been proposed [28] to perform a Laurent expansion about the complex pole. An approximation to this Laurent expansion can be obtained by decomposing the contributions of the resonant diagrams into resonant and nonresonant parts and introducing the finite width only in the former. For vertex corrections this leads to the substitution

$$\delta\mathcal{M}_{vertex}^{(s)} = -\frac{e^2M_Z^2}{c_W^2 s_W^2} \sum_{i=0,1} (\mathcal{M}_{i0}^{(s)}+\mathcal{M}_{0i}^{(s)}) \frac{F_i^{ZZH}(s)}{s-M_H^2}$$
$$\to -\frac{e^2M_Z^2}{c_W^2 s_W^2} \sum_{i=0,1} (\mathcal{M}_{i0}^{(s)}+\mathcal{M}_{0i}^{(s)}) \left[\frac{F_i^{ZZH}(M_H^2)}{s-M_H^2+iM_H\Gamma_H} \right.$$
$$\left. + \frac{F_i^{ZZH}(s)-F_i^{ZZH}(M_H^2)}{s-M_H^2} \right], \qquad (26)$$

where [to $O(\alpha)$ accuracy]

$$\Gamma_H = \text{Im}\,\Sigma^H(M_H^2)/M_H \qquad (27)$$

is the decay width of the Higgs boson. For the lowest-order and self-energy contributions we write

$$\mathcal{M}_{Born}^{(s)} + \delta\mathcal{M}_{self}^{(s)} = -\frac{e^2M_Z^2}{c_W^2 s_W^2} \mathcal{M}_{00}^{(s)} \frac{1}{s-M_H^2} \left[1 - \frac{\Sigma^H(s)}{s-M_H^2} \right]$$
$$= -\frac{e^2M_Z^2}{c_W^2 s_W^2} \mathcal{M}_{00}^{(s)} \frac{1}{s-M_H^2} \left[1 - \frac{\Sigma^H(M_H^2)}{s-M_H^2} - \Sigma'^H(M_H^2) - \frac{\Sigma^H(s)-\Sigma^H(M_H^2)-(s-M_H^2)\Sigma'^H(M_H^2)}{s-M_H^2} \right]$$
$$\to -\frac{e^2M_Z^2}{c_W^2 s_W^2} \mathcal{M}_{00}^{(s)} \left[\frac{1}{s-M_H^2+iM_H\Gamma_H} [1-\Sigma'^H(M_H^2)] - \frac{\Sigma^H(s)-\Sigma^H(M_H^2)-(s-M_H^2)\Sigma'^H(M_H^2)}{(s-M_H^2)^2} \right] \qquad (28)$$

with $\Sigma'^H(s)=d\Sigma^H(s)/ds$. We have used the fact that the renormalized Higgs-boson self-energy fulfills $\text{Re}\Sigma^H(M_H^2)=0$ and that $\text{Im}\,\Sigma^H(M_H^2)=M_H\Gamma_H$ is accounted for by the resummed terms. As the inclusion of a finite width corresponds just to the inclusion of higher-order terms, all expressions are equivalent at the one-loop level.

According to Eq. (27), Γ_H is a tree-level quantity if Σ^H is calculated at one-loop order. Consequently, in a one-loop

calculation one ends up with $O(1)$ accuracy on resonance and different treatments of the finite Higgs-boson width differ relatively in $O(\alpha)$. An improvement to $O(\alpha)$ accuracy on resonance would require to use the fully $O(\alpha)$-corrected Higgs-boson width in the resonant denominators.

The above procedure is gauge independent because we modify the amplitude by terms that depend only on the gauge-independent residue of the pole and the physical mass

and width. However, the actual application of the pole expansion deserves some care. First, the above treatment is not uniquely determined by the resonance pole, because the Laurent expansion is only applied to the form factors but not to the SME's and the split up between these two is not unique. On the other hand, the terms introduced by the modification of the amplitude in general violate the Ward identities and thus eventually unitarity. This problem could be avoided and the pole scheme could be uniquely defined by including the complete matrix elements into the Laurent expansion. This, however, leads to problems in defining the residues, i.e., in particular, the corresponding momenta and wave functions, for more general processes in certain kinematical regions (see Ref. [29]). In the following we show how one can exploit the above-mentioned freedom in the pole expansion in order to eliminate unitarity-violating terms.

We first illustrate the procedure at tree level. A general pole expansion is obtained by absorbing some arbitrary function $f(s)$ with $f(M_H^2) = 1$ into the SME $\mathcal{M}_{00}^{(s)}$ and performing the Laurent expansion for the resulting modified form factor. After resubstituting the original SME this amounts to the replacement

$$\mathcal{M}_{\text{Born}}^{(s)} \to -\frac{e^2 M_Z^2}{c_W^2 s_W^2}\, \mathcal{M}_{00}^{(s)} \left[\frac{f(s)}{s - M_H^2 + iM_H\Gamma_H} + \frac{1 - f(s)}{s - M_H^2} \right]. \tag{29}$$

The added terms are proportional to $f(s)\mathcal{M}_{00}^{(s)}\Gamma_H / (s - M_H^2)/(s - M_H^2 + iM_H\Gamma_H)$. If the matrix element $f(s)\mathcal{M}_{00}^{(s)}$

grows too fast with energy these terms violate unitarity at high energies. In the high-energy limit the ratio between the Born cross sections for longitudinal Z bosons ($LLLL$) calculated for $\Gamma_H \neq 0$ and $\Gamma_H = 0$ behaves as $1 + f(s)^2 \Gamma_H^2 / 9M_H^2$ for real $f(s)$, i.e., $f(s) = 1$ yields a result that is off by a constant factor, but for instance $f(s) = M_H^2/s$ reproduces the correct high-energy limit. While different choices of $f(s)$ by construction do not modify the resonant contribution they differ evidently in the nonresonant terms. This indefiniteness of the nonresonant lowest-order contributions gives rise to ambiguities of relative $O(\alpha)$ in the resonance region.

At the one-loop level the generalized pole expansion is obtained by absorbing arbitrary functions $f_{ij}(s)$ with $f_{ij}(M_H^2) = 1$ into the SME's $\mathcal{M}_{ij}^{(s)}$ before performing the Laurent expansion of the form factors. Besides the appearance of several functions f_{ij} such a general pole expansion even includes terms involving their derivatives f'_{ij}. For our purposes it is sufficient to consider the modified pole expansion

$$\delta\mathcal{M}_{\text{vertex}}^{(s)} \to -\frac{e^2 M_Z^2}{c_W^2 s_W^2} \sum_{i=0,1} (\mathcal{M}_{i0}^{(s)} + \mathcal{M}_{0i}^{(s)}) \left[\frac{F_i^{ZZH}(M_H^2)f(s)}{s - M_H^2 + iM_H\Gamma_H} \right.$$
$$\left. + \frac{F_i^{ZZH}(s) - F_i^{ZZH}(M_H^2)f(s)}{s - M_H^2} \right],$$

$$\mathcal{M}_{\text{Born}}^{(s)} + \delta\mathcal{M}_{\text{self}}^{(s)} \to -\frac{e^2 M_Z^2}{c_W^2 s_W^2}\, \mathcal{M}_{00}^{(s)} \left[\frac{1}{s - M_H^2 + iM_H\Gamma_H} \left[1 - \Sigma'^H(M_H^2)f(s)\right] - \frac{\Sigma^H(s) - \Sigma^H(M_H^2) - (s - M_H^2)\Sigma'^H(M_H^2)f(s)}{(s - M_H^2)^2} \right], \tag{30}$$

which differs from a consistent expansion with $f_{ij}(s) = f(s)$ only by terms of the order of Γ_H^2, i.e., $O(\alpha^2)$. If we introduce the finite width as in Eqs. (26) and (28), i.e., with $f(s) = 1$, we modify the cross section for longitudinal gauge bosons at high energies by a constant contribution of $O(\alpha \Gamma_H/M_H)$. In the modified version of the pole scheme the high-energy behavior can be improved by choosing a suitable function $f(s)$ that vanishes sufficiently fast at high energies. With our definition of the SME's (15) it is sufficient to choose $f(s) = M_H^2/s$. Note that if we did not include factors M_H^2/s to render the SME's dimensionless we would obtain a contribution to the matrix element that grows with s for $f(s) = 1$, i.e., that violates unitarity. The freedom parameterized by $f(s)$ in Eq. (30) affects the nonresonant contributions in $O(\alpha)$. On resonance this introduces ambiguities in $O(\alpha^2)$ relative to the leading resonant terms.

The above recipe for the usual on-shell renormalization scheme is directly connected with an expansion of the transition matrix element about its complex pole. In Ref. [28] such an expansion was explicitly described for angular-independent resonances, where the complications [29] in defining wave functions and momenta on resonance are absent. The procedure of Ref. [28] can be directly transferred to $ZZ \to ZZ$. In this respect only the angular-independent, i.e., the (one-particle-reducible) lowest-order, self-energy, and vertex contributions in the s channel $\mathcal{M}_{1\text{PR}}^{(s)}$, are relevant. After Dyson summation these can be written (assuming no truncation of the perturbation series) as:

$$\mathcal{M}_{1\text{PR}}^{(s)} = -\frac{e^2 M_Z^2}{c_W^2 s_W^2} t \sum_{i,j=0,1} \mathcal{M}_{ij}^{(s)} \frac{[\delta_{0i} + F_i^{ZZH}(s)][\delta_{0j} + F_j^{ZZH}(s)]}{s - M_H^2 + \Sigma^H(s)}, \tag{31}$$

i.e., as a product of full vertex functions and the full propagator. The additional SME $\mathcal{M}_{11}^{(s)}$ is defined as

$$\mathcal{M}_{11}^{(s)} = (\varepsilon_1 \cdot k_2)(\varepsilon_2 \cdot k_1)(\varepsilon_3^* \cdot k_4)(\varepsilon_4^* \cdot k_3)/s^2. \tag{32}$$

The complex pole s_p of Eq. (31) is obtained as the solution of

$$s_p - M_H^2 + \Sigma^H(s_p) = 0. \tag{33}$$

Since $\mathcal{M}_{1PR}^{(s)}$ is analytical in s, it can be continued to complex s and expanded about s_p. The leading term in this expansion is given by the resonant part

$$\mathcal{M}_{\text{reso}} = -\frac{e^2 M_Z^2}{c_W^2 s_W^2} \sum_{i,j=0,1} \mathcal{M}_{ij}^{(s)}|_{s=s_p} \frac{[\delta_{0i} + F_i^{ZZH}(s_p)][\delta_{0j} + F_j^{ZZH}(s_p)]}{(s-s_p)[1+\Sigma'^H(s_p)]}. \quad (34)$$

The residue of $\mathcal{M}_{\text{reso}}$ at the pole $1/(s-s_p)$ can be interpreted as the product of two physical amplitudes $\mathcal{M}^{H\to ZZ}$ for the decay $H\to ZZ$. To one-loop accuracy $\mathcal{M}_{1PR}^{(s)}$ can be replaced by

$$\mathcal{M}_{1PR}^{(s)} \to -\frac{e^2 M_Z^2}{c_W^2 s_W^2} \sum_{i=0,1} (\mathcal{M}_{i0}^{(s)} + \mathcal{M}_{0i}^{(s)})\left[\frac{F_i^{ZZH}(s_p)}{s-s_p} + \frac{F_i^{ZZH}(s) - F_i^{ZZH}(s_p)}{s-s_p}\right]$$

$$-\frac{e^2 M_Z^2}{c_W^2 s_W^2} \mathcal{M}_{00}^{(s)} \frac{1}{s-s_p}\left[1 - \Sigma'^H(s_p) - \frac{\Sigma^H(s) - \Sigma^H(s_p) - (s-s_p)\Sigma'^H(s_p)}{s-s_p}\right]. \quad (35)$$

Owing to $s_p = M_H^2 - iM_H\Gamma_H + O(\alpha^2)$, the right-hand side of Eq. (35) differs from Eqs. (26) and (28) only by higher-order contributions.

Note that the freedom in splitting the matrix element into SME's and form factors is also present in this approach, i.e., in Eq. (35) we could also introduce functions $f_{ij}(s)$, as described in the first part of this section. In the considered case one could avoid this ambiguity by expanding also the SME's occuring in $\mathcal{M}^{(s)}$ about s_p. However, in more complicated situations it is not always possible to include the wave functions in the pole expansion. If one then excludes the SME's from the pole expansion, as for instance advocated in Ref. [30], one is again confronted with the problem of violating Ward identities.

B. Dyson summation within the background-field method

A different approach to introduce a finite width near resonances is to Dyson sum the self-energy corrections. It is a well-known fact that in the conventional formalism Ward identities, which in particular rule the gauge cancellations, are violated if Dyson summation is applied. However, in Ref. [13] it has been shown that Dyson summation within the background-field method (BFM) (see Ref. [16], and references therein) does not violate the Ward identities if all one-particle-irreducible corrections are taken into account in the same loop order. Dyson summation naturally arranges the reducible parts of amplitudes in a way that results from forming trees with vertex functions joined by full propagators (inverse two-point functions). For the process under consideration this simply amounts to writing the (one-particle-reducible) lowest-order, self-energy, and vertex contributions in the following way:

$$\mathcal{M}_{\text{Born}} + \delta\mathcal{M}_{\text{self}} + \delta\mathcal{M}_{\text{vertex}}$$

$$\to \mathcal{M}_{1PR} = -\frac{e^2 M_Z^2}{c_W^2 s_W^2} \sum_{i,j=0,1} \sum_{r=s,t,u} \mathcal{M}_{ij}^{(r)}$$

$$\times \frac{[\delta_{0i} + F_i^{ZZH}(r)][\delta_{0j} + F_j^{ZZH}(r)]}{r - M_H^2 + \Sigma^H(r)}, \quad (36)$$

where Σ^H and F_i^{ZZH} denote the renormalized self-energy and form factors, respectively, in the BFM and

$$\mathcal{M}_{11}^{(t)} = (\varepsilon_1\cdot k_3)(\varepsilon_2\cdot k_4)(\varepsilon_3^*\cdot k_1)(\varepsilon_4^*\cdot k_2)/s^2,$$

$$\mathcal{M}_{11}^{(u)} = (\varepsilon_1\cdot k_4)(\varepsilon_2\cdot k_3)(\varepsilon_3^*\cdot k_2)(\varepsilon_4^*\cdot k_1)/s^2. \quad (37)$$

The s-channel part of Eq. (36) is formally identical to Eq. (31). Note, however, that we use Eq. (36) in the following with form factors and self-energy in finite, i.e., one-loop, order of perturbation theory.

The complete one-loop matrix element is obtained by adding the (one-particle-irreducible) box contributions and multiplying everything with the (UV-finite) wave-function renormalization factor $\sqrt{R_Z}$ for each external Z boson:

$$\mathcal{M}_{\text{BFM}} = (\mathcal{M}_{1PR} + \mathcal{M}_{\text{box}})(R_Z)^2. \quad (38)$$

Since the wave-function renormalization factor R_Z multiplies the complete matrix element, we can simply use its $O(\alpha)$ approximation

$$(R_Z)^2 = 1 - 2\,\text{Re}\,\Sigma_T'^{ZZ}(M_Z^2). \quad (39)$$

The matrix element (38) satisfies all relevant Ward identities and, in particular, does not violate unitarity at high energies. However, it depends on a gauge parameter (the quantum gauge parameter ξ_Q) via higher-order (at least two-loop) corrections which are not completely taken into account. The on-resonance self-energy is unique and equal to the physical quantity $iM_H\Gamma_H$. As a consequence, the gauge dependence is genuinely of higher order. It is crucial that in the BFM this gauge dependence cannot be enhanced by the violation of gauge cancellations because the Ward identities hold exactly even in finite orders. This is in clear contrast to the conventional formalism where tiny gauge-dependent terms can be enhanced in certain kinematical configurations. Therefore, the BFM yields at least a practical solution for the description of resonances in gauge theories as long as one avoids pathological gauges such as the unitary gauge ($\xi_Q\to\infty$), which may lead to an enhancement of the gauge-parameter-dependent terms by the artificially introduced large scale ξ_Q. The higher-order gauge dependence is nothing but a result of the fact that a Dyson summation is always

arbitrary to some extent. For gauge parameters of order one it merely gives rise to higher-order uncertainties which are anyhow present in every finite-order calculation.

In the conventional formalism the matrix element after Dyson summation depends not only on the gauge but in addition on the choice of the field renormalization. In the BFM the matrix element is actually independent of the field renormalization. This can be seen as follows. The field renormalization is fixed by background field gauge invariance up to a UV-finite linear transformation of the renormalized fields. Such a linear transformation turns the linear Ward identities for the background-field vertex functions into Ward identities for transformed vertex functions with the same structure. These modified Ward identities are still exactly valid even

for full, i.e., Dyson-summed, propagators. However, the effects of the linear transformation cancel in S-matrix elements, thus giving a unique answer.

The resonant part of the Dyson-summed one-loop matrix element (36) in the BFM reads, for $s = M_H^2$,

$$\mathcal{M}_{\mathrm{BFM}}\big|_{s=M_H^2} \approx - \frac{e^2 M_Z^2}{c_W^2 s_W^2} (R_Z)^2 \sum_{i,j=0,1} \mathcal{M}_{ij}^{(s)}$$
$$\times \frac{[\delta_{0i} + F_i^{ZZH}(M_H^2)][\delta_{0j} + F_j^{ZZH}(M_H^2)]}{i M_H \Gamma_H}. \quad (40)$$

This differs from the resonant part of the pole-scheme amplitude (30):

$$\mathcal{M}_{\mathrm{pole}}\big|_{s=M_H^2} \approx - \frac{e^2 M_Z^2}{c_W^2 s_W^2} \frac{\mathcal{M}_{00}^{(s)}[1 - \Sigma'^H(M_H^2)] + \Sigma_{i=0,1}(\mathcal{M}_{i0}^{(s)} + \mathcal{M}_{0i}^{(s)}) F_i^{ZZH}(M_H^2)}{i M_H \Gamma_H}, \quad (41)$$

in $O(\alpha)$ in relative terms, in accordance with the discussion after Eq. (27). Moreover, Eq. (40) is even gauge dependent in this order on resonance, whereas Eq. (41) is manifestly gauge independent. The bulk of these effects can be attributed to the contribution of $\Sigma'^H(M_H^2)$ and thus to the different wave-function renormalization in the BFM.

In order to obtain the cross section on resonance also in $O(\alpha)$ accuracy the imaginary part of the Higgs-boson self-energy has to be included in two-loop order. In the pole scheme this is equivalent to the introduction of the $O(\alpha)$-corrected Higgs-boson width in the propagator. However, in the BFM approach all two-loop corrections are required in order to preserve the Ward identities.

VI. CROSS SECTION FOR LONGITUDINAL Z BOSONS FROM THE EQUIVALENCE THEOREM

The corrections of $O(\alpha M_H^2 / s_W^2 M_W^2)$ to longitudinal gauge-boson scattering processes have been calculated in the literature [3,4,7,8] using the ET [9–13], which relates amplitudes involving longitudinal gauge bosons with those involving the associated would-be Goldstone bosons in the high-energy limit. Because the latter amplitudes are much easier to be calculated, the ET was frequently used to obtain cross sections in the high-energy limit.

A. Equivalence theorem within the background-field method

When using the ET in higher-order calculations one has to be careful to include all correction factors that result from renormalization and amputation [11]. It has been found in Ref. [13] that this is particularly easy within the BFM. In this formalism the matrix elements for external longitudinal vector bosons are directly obtained from the amputated Green functions with the corresponding would-be Goldstone boson fields multiplied with the wave-function renormalization constants of the gauge bosons. Moreover, in contrast to the conventional formalism, in the BFM the ET is valid with and without Dyson summation.

B. Results for $Z_L Z_L \rightarrow Z_L Z_L$

We want to apply the ET to the process $Z_L Z_L \rightarrow Z_L Z_L$ in the framework of the BFM and investigate the accuracy of the corresponding predictions.

To this end we have to consider the process $\chi\chi \rightarrow \chi\chi$, where χ is the would-be Goldstone boson associated with the Z boson. In lowest order the four diagrams of Fig. 10 yield

$$\mathcal{M}_{\mathrm{Born}}^{\chi\chi\rightarrow\chi\chi} = - \frac{e^2 M_H^2}{4 s_W^2 c_W^2 M_Z^2} \left[3 + \frac{M_H^2}{s - M_H^2} + \frac{M_H^2}{t - M_H^2} + \frac{M_H^2}{u - M_H^2} \right]. \quad (42)$$

For $s \gg M_Z^2$ the matrix element for $Z_L Z_L \rightarrow Z_L Z_L$ approaches the one for $\chi\chi \rightarrow \chi\chi$ for any value of M_H [12]. We note that this agreement is destroyed if one includes the finite Higgs-boson width in the way discussed in Sec. V A without expanding also the SME's or appropriately adjusting the function $f(s)$ in Eq. (29).

Following the treatment of Sec. V B, the matrix element for $\chi\chi \rightarrow \chi\chi$ including $O(\alpha)$ corrections is given similarly to Eq. (38) by

$$\mathcal{M}^{\chi\chi\rightarrow\chi\chi} = \left(\mathcal{M}_{1\mathrm{PR}}^{\chi\chi\rightarrow\chi\chi} - 3\frac{e^2 M_H^2}{4 s_W^2 c_W^2 M_Z^2} + \mathcal{M}_{\mathrm{box}}^{\chi\chi\rightarrow\chi\chi} \right)(R_Z)^2 \quad (43)$$
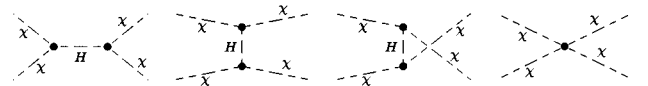
with

FIG. 10. Lowest-order diagrams for $\chi\chi \rightarrow \chi\chi$.

$$\mathcal{M}_{1PR}^{\chi\chi\rightarrow\chi\chi}=-\frac{e^2 M_H^4}{4 c_W^2 s_W^2 M_Z^2}$$

$$\times\sum_{r=s,t,u}\frac{[1+F^{\chi\chi H}(r)][1+F^{\chi\chi H}(r)]}{r-M_H^2+\Sigma^H(r)}. \tag{44}$$

Because $\mathcal{M}_{1PR}^{\chi\chi\rightarrow\chi\chi}$ vanishes for $s\gg M_H^2$ as M_H^2/s, the boxes dominate the matrix element for $\chi\chi\rightarrow\chi\chi$ at high energies. The matrix elements for $\chi\chi\rightarrow\chi\chi$ are calculated in exactly the same way as for $ZZ\rightarrow ZZ$. In contrast to $ZZ\rightarrow ZZ$ the one-loop corrections to $\chi\chi\rightarrow\chi\chi$ possess a transparent form; they are explicitly presented in Appendix B. We recall that the usage of the BFM is crucial for the ET to work for Dyson-summed amplitudes. Because the would-be Goldstone bosons are scalars, no polarization vectors and no SME's occur, and no unitarity cancellations between individual contributions take place. This simplifies the calculation considerably.

The Higgs-boson resonance can be treated exactly as for $ZZ\rightarrow ZZ$. Since the wave functions are trivial constants, and thus no split into SME's and invariant functions is necessary, the ambiguity in applying the pole expansion is absent.

In order to improve the accuracy of a calculation via the ET one can combine the full lowest-order matrix element with the $O(\alpha)$ corrections from $\chi\chi\rightarrow\chi\chi$ resulting in

$$\mathcal{M}_{\text{mixed}}=\mathcal{M}_{\text{Born}}^{Z_L Z_L\rightarrow Z_L Z_L}+\delta\mathcal{M}_{\text{one loop}}^{\chi\chi\rightarrow\chi\chi}. \tag{45}$$

This treatment is, however, not possible if one uses Dyson summation, because in this case the lowest-order matrix element cannot be linearly separated from the one-loop corrections.

C. Heavy-Higgs-boson effects

In the literature an approximation for the matrix element $\mathcal{M}^{\chi\chi\rightarrow\chi\chi}$ by the leading contributions for s, $M_H^2\gg M_Z^2$ was frequently used [3–8]. In this approximation the building blocks of Eqs. (43) and (44) take a particularly simple form. In the BFM we find, in this limit,

$$\Sigma^H(r)=\frac{\alpha}{4\pi}\frac{M_H^2}{8 s_W^2 M_W^2}\{3M_H^2[3B_0(r,M_H,M_H)+B_0(r,0,0)$$

$$-3B_0(M_H^2,M_H,M_H)-\text{Re}\{B_0(M_H^2,0,0)\}]\}$$

$$+\delta Z_{\hat{H}}(r-M_H^2),$$

$$F^{\chi\chi H}(r)=-\frac{\alpha}{4\pi}\frac{M_H^2}{8 s_W^2 M_W^2}\bigg\{2M_H^2[3C_0(r,0,0,M_H,M_H,0)$$

$$+C_0(r,0,0,0,0,M_H)]+3B_0(r,M_H,M_H)$$

$$+5B_0(r,0,0)+4B_0(0,0,M_H)$$

$$-9B_0(M_H^2,M_H,M_H)-3\,\text{Re}\{B_0(M_H^2,0,0)\}-\frac{1}{2}\bigg\}$$

$$+\frac{1}{2}\,\delta Z_{\hat{H}}+\delta Z_{\hat{\chi}},$$

$$\mathcal{M}_{\text{box}}^{\chi\chi\rightarrow\chi\chi}=\alpha^2\frac{M_H^4}{32 s_W^4 M_W^4}\{2M_H^4[D_0(0,0,0,0,s,t,M_H,0,M_H,0)$$

$$+D_0(0,0,0,0,s,t,0,M_H,0,M_H)]$$

$$+4M_H^2[C_0(s,0,0,M_H,M_H,0)$$

$$+3C_0(s,0,0,0,0,M_H)]+B_0(s,M_H,M_H)$$

$$+11B_0(s,0,0)-9B_0(M_H^2,M_H,M_H)$$

$$-3\,\text{Re}\{B_0(M_H^2,0,0)\}-1+(s\rightarrow t,t\rightarrow u)$$

$$+(s\rightarrow u,t\rightarrow s)\}+2\delta Z_{\hat{\chi}},$$

$$R_Z=1, \tag{46}$$

where B_0, C_0, and D_0 are scalar one-loop functions [18,22]. The wave-function renormalization constants read, in the BFM,

$$\delta Z_{\hat{H}}=\delta Z_{\hat{\chi}}=-\frac{\alpha}{4\pi}\frac{M_H^2}{8 s_W^2 M_W^2}. \tag{47}$$

The above results are in agreement with those of Ref. [6]. Since the approximation (46) merely involves corrections of $O(\alpha M_H^2/s_W^2 M_W^2)$, it follows from power counting (see Ref. [12], and references therein) that only diagrams with internal scalar lines contribute. We note in passing that the terms of $O(\alpha M_H^2/s_W^2 M_W^2)$ originate entirely from the SU(2) sector of the SM, i.e., they could also be obtained from the corresponding reaction $W^3 W^3\rightarrow W^3 W^3$ in the pure SU(2) gauge theory.

We have checked that in the limit $M_Z^2\ll s\ll M_H^2$ the amplitude $\mathcal{M}^{\chi\chi\rightarrow\chi\chi}$ reduces to

$$\mathcal{M}^{\chi\chi\rightarrow\chi\chi}=\sum_{r=s,t,u}\frac{\alpha^2 r^2}{16 s_W^4 M_W^4}\left[\ln\left(\frac{M_H^2}{-r-i\varepsilon}\right)+\frac{3\sqrt{3}\,\pi}{2}-\frac{26}{3}\right], \tag{48}$$

as already given in Refs. [3, 4]. In this context we remark that the result (48) can be most easily obtained from the general structure of the heavy-Higgs-boson limit of the SM. The matrix element $\mathcal{M}^{\chi\chi\rightarrow\chi\chi}$ (48) gets contributions only from $\mathcal{L}_4$ and $\mathcal{L}_5$ of the effective Lagrangian of Ref. [31], which quantifies the heavy Higgs-boson effects, and from the (three) irreducible graphs in the gauged nonlinear σ model which contain only quartic scalar couplings.

VII. DISCUSSION OF NUMERICAL RESULTS

A. Computational details

For the calculations we use the following parameter set [32]:

$$\alpha^{-1}=137.035\,989\,5, \quad M_Z=91.188\text{ GeV},$$

$$M_W=80.26\text{ GeV}, \quad m_e=0.510\,999\,06\text{ MeV},$$

$$m_u=47.0\text{ MeV}, \quad m_d=47.0\text{ MeV},$$

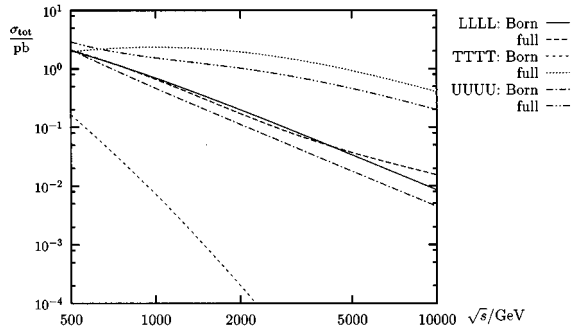$$m_\mu=105.658\,389\text{ MeV}, \quad m_c=1.55\text{ GeV},$$

FIG. 11. Lowest-order and corrected integrated cross sections for various polarizations at $M_H = 100$ GeV.

$$m_s = 150 \text{ MeV}, \quad m_T = 1771.1 \text{ MeV},$$

$$m_t = 180 \text{ GeV}, \quad m_b = 4.5 \text{ GeV}. \tag{49}$$

The masses of the light quarks are adjusted such that the experimentally measured hadronic vacuum polarization is reproduced [33]. For a Higgs-boson with a mass of $M_H = 700$ GeV these parameters yield the lowest-order decay width $\Gamma_H \approx 175.29$ GeV, i.e., about one fourth of the mass.

The various independent calculations described in Sec. IV A agree numerically typically to ~ 10 digits apart from the regions close to the boundaries of phase space. At these boundaries the reduction of tensor integrals to scalar integrals breaks down. We avoid these regions by using the angular cut $\theta_{\text{cut}} = 10°$, which also removes the Landau singularities in the fermionic boxes for energies above about 500 GeV.

B. Corrected cross sections

The integrated cross sections for unpolarized, purely transverse, and purely longitudinal Z bosons in lowest order and including the one-loop corrections are shown in Figs. 11 and 12 for $M_H = 100$ GeV and $M_H = 700$ GeV, respectively (repeating information from Figs. 2, 3, 7, and 8). In the case of $M_H = 100$ GeV no finite Higgs-boson width is introduced; for $M_H = 700$ GeV we apply Dyson summation within the BFM using the renormalization scheme of Ref. [16]. The Higgs-boson-mass dependence of the cross section for purely transverse Z bosons is below 10% including the Higgs-
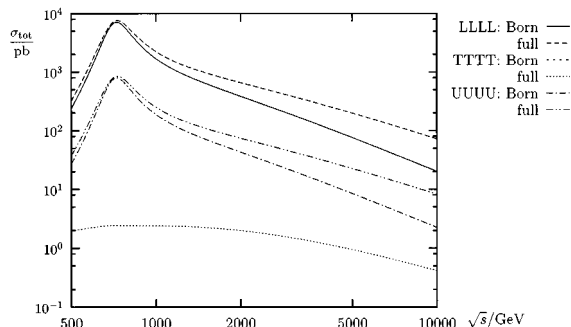

FIG. 12. Lowest-order and corrected integrated cross sections for various polarizations at $M_H = 700$ GeV. (The lowest-order $TTTT$ cross section is not visible.)

boson-resonance effects. The corresponding lowest-order cross section is very small at high energies and not visible in Fig. 12.

The differential cross sections for various energies are shown in Figs. 13 and 14. For small energies the angular variation of the cross sections stays within one order of magnitude. For high energies and a small Higgs-boson mass the corrected cross sections are strongly peaked in the forward and backward directions, while the lowest-order cross sections are relatively flat in the considered angular region. The cross section for purely longitudinal gauge bosons has kinematical zeros if $M_H \lesssim \sqrt{1 + \sqrt{3}} M_Z \approx 150$ GeV, which move towards the forward and backward directions with increasing energy. For a large Higgs-boson mass the cross section for purely longitudinal Z bosons, which dominates in this regime, becomes flat and therefore also the unpolarized cross section.

C. Higgs-boson resonance

In Figs. 15 and 16 we compare several different treatments of the Higgs-boson resonance using $M_H = 700$ GeV. We include the lowest-order (Born, $\Gamma_H = 0$) and the corrected (full, $\Gamma_H = 0$) cross sections for vanishing Higgs-boson width for reference. We show the lowest-order (Born, pole scheme) and the corrected (full, pole scheme) cross section in the pole-scheme treatment given in Eqs. (26) and (28) as well as the corrected cross section in the modified pole scheme (full, mod. pole scheme) according to Eq. (30) with $f(s) = M_H^2/s$. In addition we give the cross sections resulting from Dyson summation according to Eqs. (36) and (38) in the BFM (BFM, Dyson) and the corresponding one in the conventional formalism (conv., Dyson). Apart from the Dyson-summed cross sections all others are identical in the BFM and in the conventional formalism. Since the unpolarized cross section is dominated by the one for purely longitudinal Z bosons for a large Higgs-boson mass, Fig. 15 holds essentially also for the latter cross section after multiplying by a factor 9.

The crucial differences between the various treatments can already be seen in Fig. 15, which shows the integrated cross section. Owing to the crude resolution the pole-scheme cross sections with or without $O(\alpha)$ corrections cannot be separated from the corresponding cross sections for $\Gamma_H = 0$ at high energies. The deviation of the Dyson-summed BFM cross section is due to higher-order corrections that become increasingly important with energy. The Dyson-summed conventional cross section deviates more for energies above a few TeV and becomes completely wrong for energies higher than 10 TeV. This results from the violation of the Ward identities which leads to unitarity violation at high energies.

The differences between the various treatments of the Higgs-boson resonance can be seen more clearly in Fig. 16, where the corrected cross sections are shown normalized to the one in the modified pole scheme. The difference between the pole scheme and the modified pole scheme is below 2% and becomes small at high energies. Note, however, that by using dimensionful SME's the pole-scheme cross sections could become completely wrong at high energies owing to spurious unitarity-violating terms.
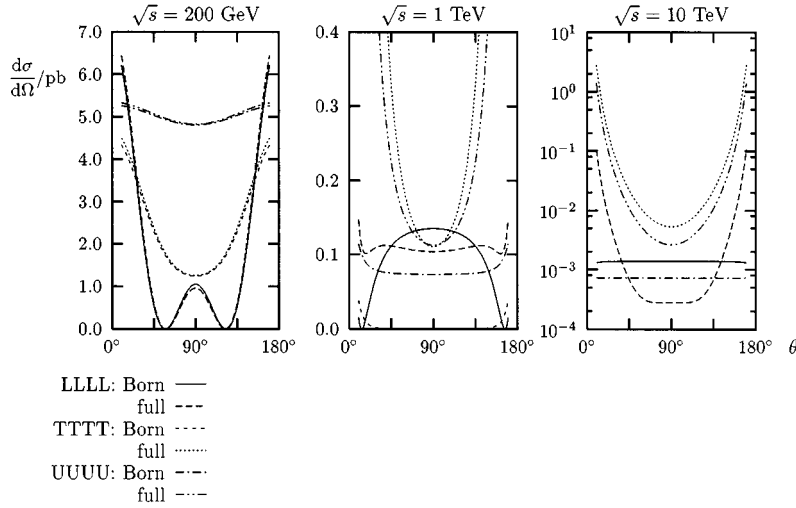
FIG. 13. Lowest-order and corrected differential cross sections for various polarizations and c.m.s. energies at $M_H = 100$ GeV.

In the resonance region the Dyson-summed cross sections deviate from the cross sections in the modified pole scheme by up to 19 and 7 % in the BFM and the conventional formalism, respectively. This difference is due to the fact that our calculation near the resonance is only of $O(1)$ accuracy since the lowest-order contribution in the resonance denominator vanishes on resonance (see Sec. V A). The size of these differences and the correction of 24% of the pole scheme calculation on resonance set the typical scale for the missing $O(\alpha)$ corrections in the resonance region.

D. The cross section for $Z_L Z_L \rightarrow Z_L Z_L$ and the equivalence theorem

Finally, we want to investigate the numerical accuracy of the ET. We distinguish the cases without and with a Higgs-boson resonance. In Fig. 17 we consider the case of no Higgs-boson resonance ($M_H = 100$ GeV). We show the lowest-order cross section (Born) calculated from the ET normalized to the lowest-order cross section for $Z_L Z_L \rightarrow Z_L Z_L$, the fully corrected cross section (full) calculated from the ET and the cross section obtained from the matrix element (45) (mixed) both normalized to the fully corrected cross section for $Z_L Z_L \rightarrow Z_L Z_L$. The quality of the ET at $E_{c.m.s.} = 1$ TeV (2 TeV) is about 17% (5%) for the lowest order, 24% (10%) for one-loop, and 6% (4%) for one-loop mixed. As expected, the one-loop mixed approximation is substantially better than the simple ET cross section.

In Fig. 18 we investigate the accuracy of the ET in the

presence of a Higgs-boson resonance at $M_H = 700$ GeV. We show again the ratios of the lowest-order and corrected cross sections obtained using the ET and from the direct calculation. In the lowest-order cross section we include the finite width naively (Born) and in the modified pole scheme (mod. Born) (29). The lowest-order cross section from the ET approaches that of the modified pole scheme at high energies. Including the finite width naively leads to a cross section that deviates at high energies from these two cross sections by a factor $1 + \Gamma_H^2 / 9 M_H^2 \approx 1.007$ for $M_H = 700$ GeV (see Sec. V A). For the corrected cross sections we have applied Dyson summation within the BFM. Because of the Dyson summation the mixed case does not make sense anymore. Instead we show the cross section resulting from the $O(\alpha M_H^2 / s_W^2 M_W^2)$ approximation of the RC's (46) normalized to the fully corrected cross section for $Z_L Z_L \rightarrow Z_L Z_L$. The ET works much better for a heavy Higgs boson. At $E_{c.m.s.} = 1$ TeV (2 TeV) we now find a deviation of 8% (2%) for the lowest order [using the modified Born according to Eq. (29)] and 6% (2%) for the corrected cross section. For energies above 2 TeV the deviation between the corrected cross sections is practically equal to the deviation between the lowest-order cross sections. The $O(\alpha M_H^2 / s_W^2 M_W^2)$ approximation (46) works well in the regime $M_Z^2 \ll M_H^2 \ll s \ll M_H^4 / M_Z^2$, where the upper limit for the energy results from the neglect of corrections proportional to s / M_Z^2 with respect to the ones proportional to M_H^4 / M_Z^4. For $M_H = 700$ GeV this restricts the energy to $\sqrt{s} \sim 1 - 3$ TeV, which is nicely reflected in the figure.
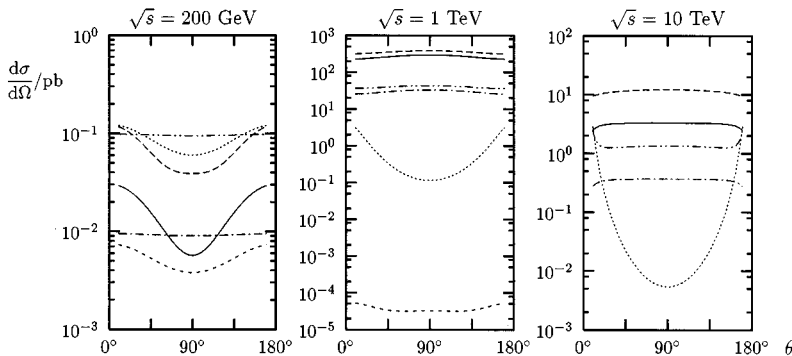

FIG. 14. Lowest-order and corrected differential cross sections for various polarizations (as indicated in Fig. 13) and c.m.s. energies at $M_H = 700$ GeV.
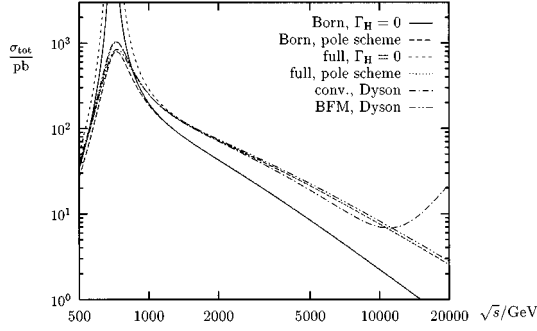
FIG. 15. Integrated unpolarized cross section at $M_H = 700$ GeV for various treatments of the Higgs-boson resonance.

VIII. CONCLUSIONS

Owing to the strong sensitivity to the gauge-boson and scalar self-interactions, scattering of massive gauge bosons found continuous interest in the literature, where the emphasis was directed to strong-coupling effects for longitudinally polarized gauge bosons. We have supplemented the existing results for the enhanced radiative corrections of order $O(\alpha M_H^2 / s_W^2 M_W^2)$ by the complete $O(\alpha)$ corrections to $ZZ \rightarrow ZZ$ for arbitrarily polarized Z bosons.

At high energies the radiative corrections are found to be large, at several TeV they are typically of the order of the lowest-order cross sections. Whereas the cross section for purely transverse Z bosons at high energies is totally negligible in lowest order, the corrections enhance this cross section such that it becomes one of the dominating channels.

The introduction of a finite Higgs-boson width in order to describe the resonance well is a nontrivial task. We have compared different approaches, viz., different variants of the Laurent expansion about the complex pole and the Dyson summation of self-energies, where the latter has been performed both in the conventional formalism as well as in the background-field formalism. From a theoretical point of view, the background-field approach is the most convincing one, since it naturally guarantees a reasonable cross section also far above the resonance, where the validity of Ward identities is crucial to imply the necessary gauge cancellations. However, in order to obtain a relative precision of $O(\alpha)$ on resonance one would have to perform a complete two-loop calculation. In order to obtain the same precision on resonance in the pole scheme only the imaginary part of

the self-energy has to be evaluated at two loops. However, as the pole scheme and the other mentioned methods do not care about the Ward identities, theoretical uncertainties may get out of control in the presence of gauge cancellations. Using the pole scheme carelessly can lead to unitarity-violating terms at high energies, and Dyson summation within the conventional formalism in fact yields a totally wrong cross section in the high-energy limit.

We have investigated longitudinal Z-boson scattering $Z_L Z_L \rightarrow Z_L Z_L$ in more detail and performed a complete $O(\alpha)$ calculation using the Goldstone-boson equivalence theorem. For a center-of-mass energy of 1 TeV (2 TeV) the deviation of the equivalence theorem from the exact $O(\alpha)$ result is about 24% (10%) and 6% (2%) for a Higgs-boson mass M_H of 100 GeV and 700 GeV, respectively, with an asymptotic approach in the high-energy limit. The frequently used approximation by the enhanced corrections of $O(\alpha M_H^2 / s_W^2 M_W^2)$ for a heavy Higgs boson is good for energies of a few TeV but gets worse with increasing energy.

Although Z-boson scattering is the simplest representative of massive gauge-boson scattering, it contains the typical features such as the Higgs-boson resonance and enhanced heavy-Higgs-boson corrections. In contrast to other gauge-boson scattering processes, the lowest-order cross sections for transverse Z-boson scattering are suppressed and no real photon radiation needs to be considered in $ZZ \rightarrow ZZ$. Nevertheless, we expect that our results at least qualitatively carry over to the other massive gauge-boson scattering reactions.
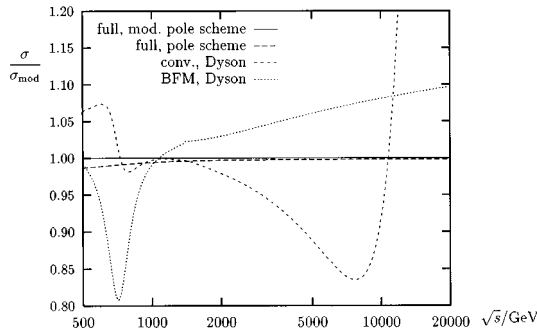
FIG. 16. Relative deviation of various treatments of the Higgs-boson resonance from the modified pole-scheme result for the integrated unpolarized cross section at $M_H = 700$ GeV.
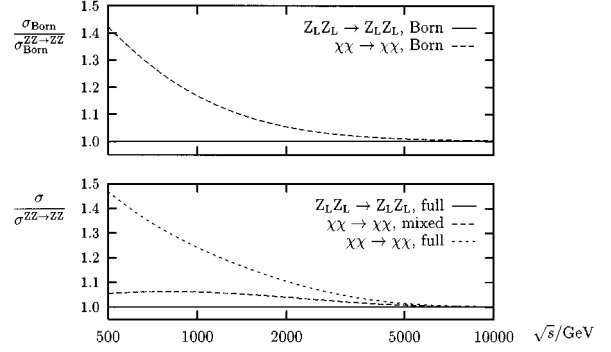

FIG. 17. Relative deviations of the ET predictions for $Z_L Z_L \rightarrow Z_L Z_L$ at $M_H = 100$ GeV.
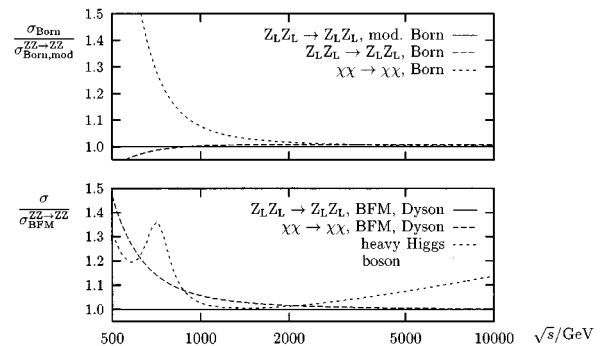

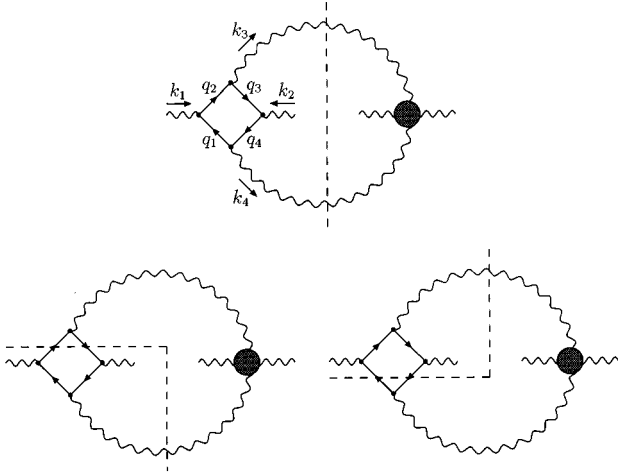FIG. 18. Relative deviations of the ET predictions for $Z_L Z_L \rightarrow Z_L Z_L$ at $M_H = 700$ GeV.

FIG. 19. Generic form of some singular contributions to $ZZ \rightarrow Zf\bar{f}$, which are related by cutting rules.

APPENDIX A: DISCUSSION OF THE LANDAU SINGULARITY IN BOX DIAGRAMS

In Sec. IV D we briefly discussed the Landau singularity which occurs in some fermionic box diagrams if the fermion mass m fulfills $m < M_Z/2$. Although we have argued that this singularity is unphysical and only caused by the use of the equivalent vector-boson approximation for pp or ee collisions, it is nevertheless interesting to investigate some formal properties of the singularity.

From general considerations (e.g., about unitarity) one expects that the singularity drops out in the fully inclusive cross section, i.e., if all possible final states are taken into account. We have verified this compensation by explicitly calculating the singular contributions of Fig. 19 to the inclusive cross section $ZZ \rightarrow 4f$. The shaded circle in Fig. 19 represents any regular graph for $ZZ \rightarrow ZZ$, i.e., only the cuts that are explicitly shown in Fig. 19 are relevant for the singular contributions. If the shaded circle also contains the singularity more cuts have to be considered. We restrict ourselves to the case where the produced Z bosons are on their mass shell, $k_3^2 = k_4^2 = M_Z^2$.

The singularity in the loop integral of the upper graph of Fig. 19 stems from integration momenta $q_1 \sim \hat{q}$ with

$$\hat{q}^{\mu} = -\frac{1}{2}(k_1 - k_3)^{\mu} + \frac{t - 2M_Z^2}{2s}(k_3 + k_4)^{\mu}, \quad \hat{q}^2 = \frac{4M_Z^4 - tu}{4s},$$

$$(A1)$$

and occurs for $\hat{q}^2 \rightarrow m^2$, which follows from the Landau equations for the integral. Thus, the singular contribution of the virtual graph is simply obtained by setting $q_1 \rightarrow \hat{q}$ in the numerator such that the remaining integral is proportional to the D_0 function, the singular contribution of which is given in Eq. (21).

The singular contributions in the lower graphs of Fig. 19 occur in the phase-space integrals of the produced fermion-antifermion pair and can be obtained from the corresponding scalar integrals analogously to the loop integral. For instance the relevant scalar integral for the lower left graph is given by

$$I = \int \frac{d^3\mathbf{k}}{(2\pi)^3 2k^0} \int \frac{d^3\mathbf{k}'}{(2\pi)^3 2k'^0} (2\pi)^4 \delta^{(4)}(k_3 - k - k')$$

$$\times \frac{1}{(q_1^2 - m^2 + i\varepsilon)(q_4^2 - m^2 + i\varepsilon)}, \quad (A2)$$

where

$$q_1 = k - k_1, \quad q_4 = k - k_1 + k_4 = k_2 - k', \quad k^2 = k'^2 = m^2.$$

$$(A3)$$

Inspection of the Landau equations for I reveals that the singularity in I originates from a point in phase space where the fermion momenta $\mathbf{k}$ and $\mathbf{k}'$ are coplanar with the scattering plane spanned by the $\mathbf{k}_l$. Explicit calculation yields

$$I|_{\text{sing}} = -\frac{i}{16\pi^2} D_0|_{\text{sing}}, \quad (A4)$$

which is also valid for the corresponding scalar integral for the lower right graph of Fig. 19.

The relation between the singular contributions of D_0 and I guarantees the cancellation of the singularity in the sum of the graphs of Fig. 19 if the produced Z bosons are on shell. However, the cancellation in general is incomplete if individual flavors or spins in the fermionic final state are observed or if phase-space cuts are applied.

Therefore, we conclude that a careful analysis of the actual physical realization of the underlying process is mandatory if such singularities appear for physical situations. For the subprocess $ZZ \rightarrow ZZ$ this means that one has to go one step back and to consider the full reaction including the production mechanism of the incoming Z bosons in more detail.

APPENDIX B: ONE-LOOP CORRECTIONS TO $\chi\chi \rightarrow \chi\chi$

In Sec. VI C we explicitly gave the leading corrections to longitudinal Z-boson scattering in the limit s, $M_H^2 \gg M_Z^2$. More generally, the complete corrections to $\chi\chi \rightarrow \chi\chi$ also take a relatively simple form in contrast with the formulas for $Z_L Z_L \rightarrow Z_L Z_L$:

$$\Sigma^H(r) = \frac{\alpha}{4\pi} \frac{1}{8 s_W^2 M_W^2} \left\{ 9M_H^4 B_0(r, M_H, M_H) + 2(M_H^4 + 4M_H^2 M_W^2 + 12M_W^4 - 8rM_W^2)B_0(r, M_W, M_W) + (M_H^4 + 4M_H^2 M_Z^2 + 12M_Z^4 \right.$$

$$- 8rM_Z^2)B_0(r, M_Z, M_Z) + 3M_H^4 B_0(0, 0, M_H) + 2M_W^2(M_H^2 + 6M_W^2)B_0(0, 0, M_W) + M_Z^2(M_H^2 + 6M_Z^2)B_0(0, 0, M_Z)$$

$$\left. - 24M_W^4 - 12M_Z^4 + \sum_f 4N_f^c m_f^2[(r - 4m_f^2)B_0(r, m_f, m_f) - 2m_f^2 B_0(0, 0, m_f)] \right\} - \delta M_H^2 + \delta Z_{\hat{H}}(r - M_H^2),$$

$$F^{\chi\chi H}(r) = -\frac{\alpha}{4\pi}\frac{1}{8s_W^2 M_H^2 M_W^2}\Bigg\{6M_H^2[(M_H^2-M_Z^2)^2+2M_Z^2(r-2M_Z^2)]C_0(r,M_Z^2,M_Z^2,M_H,M_H,M_Z)$$

$$+2(M_H^6-3M_H^2 M_Z^4-6M_Z^6+4rM_H^2 M_Z^2)C_0(r,M_Z^2,M_Z^2,M_Z,M_Z,M_H)+8M_W^2(M_H^2+4M_W^2)(r-2M_Z^2)$$

$$\times C_0(r,M_Z^2,M_Z^2,M_W,M_W,M_W)+3M_H^2(M_H^2+2M_Z^2)B_0(r,M_H,M_H)+2(M_H^4+4M_H^2 M_W^2+12M_W^4)B_0(r,M_W,M_W)$$

$$+(3M_H^4+6M_H^2 M_Z^2+8M_Z^4)B_0(r,M_Z,M_Z)+4(M_H^2-M_Z^2)^2 B_0(M_Z^2,M_H,M_Z)-16M_W^4-8M_Z^4$$

$$+\sum_f 8N_f^c m_f^4[(2M_Z^2-r)C_0(r,M_Z^2,M_Z^2,m_f,m_f,m_f)-2B_0(r,m_f,m_f)]\Bigg\}$$

$$+\delta Z_e-\frac{\delta s_W^2}{2s_W^2}-\frac{\delta M_W^2}{2M_W^2}+\frac{\delta M_H^2}{M_H^2}+\frac{e}{2s_W}\frac{\delta t}{M_W M_H^2}+\frac{1}{2}\delta Z_{\hat H}+\delta Z_{\hat\chi},$$

$$\mathcal{M}^{\chi\chi\to\chi\chi}_{\text{box}}=\alpha^2\frac{1}{32s_W^4 M_W^4}\Bigg\{2[(M_H^2-M_Z^2)^2+2M_Z^2(s-2M_Z^2)]^2 D_0(M_Z^2,M_Z^2,M_Z^2,M_Z^2,s,t,M_H,M_Z,M_H,M_Z)+2[(M_H^2-M_Z^2)^2$$

$$+2M_Z^2(t-2M_Z^2)]^2 D_0(M_Z^2,M_Z^2,M_Z^2,M_Z^2,t,s,M_H,M_Z,M_H,M_Z)+16M_W^4[(s-2M_Z^2)^2+(t-2M_Z^2)^2]$$

$$\times D_0(M_Z^2,M_Z^2,M_Z^2,M_Z^2,s,t,M_W,M_W,M_W,M_W)+4(M_H^2+2M_Z^2)[(M_H^2-M_Z^2)^2+2M_Z^2(s-2M_Z^2)]$$

$$\times C_0(s,M_Z^2,M_Z^2,M_H,M_H,M_Z)+4[3M_H^2(M_H^2-M_Z^2)^2+4M_Z^4(s-2M_Z^2)]C_0(s,M_Z^2,M_Z^2,M_Z,M_Z,M_H)$$

$$+16M_W^2(M_H^2+4M_W^2)(s-2M_Z^2)C_0(s,M_Z^2,M_Z^2,M_W,M_W,M_W)+(M_H^2+2M_Z^2)^2 B_0(s,M_H,M_H)$$

$$+2(M_H^4+4M_H^2 M_W^2+12M_W^4)B_0(s,M_W,M_W)+(9M_H^4+8M_Z^4)B_0(s,M_Z,M_Z)-16M_W^4-8M_Z^4$$

$$+\sum_f 4N_f^c m_f^4[(st-2M_Z^4)D_0(M_Z^2,M_Z^2,M_Z^2,M_Z^2,s,t,m_f,m_f,m_f,m_f)+4(2M_Z^2-s)C_0(s,M_Z^2,M_Z^2,m_f,m_f,m_f)$$

$$-4B_0(s,m_f,m_f)]+(s\to t,t\to u)+(s\to u,t\to s)\Bigg\}+2\delta Z_e-\frac{\delta s_W^2}{s_W^2}-\frac{\delta M_W^2}{M_W^2}+\frac{\delta M_H^2}{M_H^2}+\frac{e}{2s_W}\frac{\delta t}{M_W M_H^2}+2\delta Z_{\hat\chi},\quad \text{(B1)}$$

where the sum over f extends over all fermion flavors, and N_f^c denotes the color factor for the fermion f. The scalar four-point function is defined as $(p_1+p_2+p_3+p_4=0)$

$$D_0[p_1^2,p_2^2,p_3^2,p_4^2,(p_1+p_2)^2,(p_2+p_3)^2,m_1,m_2,m_3,m_4]$$

$$=\int\frac{d^4q}{i\pi^2}\frac{1}{(q^2-m_1^2)[(q+p_1)^2-m_2^2][(q+p_1+p_2)^2-m_2^2][(q-p_4)^2-m_2^2]}.\quad\text{(B2)}$$

Note that these results are derived within the BFM and include the heavy-Higgs-boson corrections of Eq. (46) as special case. For the sake of simplicity the explicit expressions for the counterterms are left open; they are easily calculated in the renormalization scheme of Ref. [16].

---

[1] D. A. Dicus and V. S. Mathur, Phys. Rev. D **7**, 3111 (1973).

[2] B. W. Lee, C. Quigg, and H. B. Thacker, Phys. Rev. D **16**, 1519 (1977).

[3] G. Passarino, Phys. Lett. **156B**, 231 (1985); Nucl. Phys. **B343**, 31 (1990); M. Veltman and F. Yndurain, *ibid.* **B325**, 1 (1989).

[4] S. Dawson and S. Willenbrock, Phys. Rev. Lett. **62**, 1232 (1989); Phys. Rev. D **40**, 2880 (1989).

[5] W. Marciano, G. Valencia, and S. Willenbrock, Phys. Rev. D **40**, 1725 (1989); L. Durand, J. M. Johnson, and J. L. Lopez, Phys. Rev. Lett. **64**, 1215 (1990); Phys. Rev. D **45**, 3112 (1992).

[6] L. Durand, J. M. Johnson, and P. N. Maher, Phys. Rev. D **44**, 127 (1991); T. N. Truong, Phys. Lett. B **258**, 402 (1991).

[7] S. N. Gupta, J. M. Johnson, and W. W. Repko, Phys. Rev. D **48**, 2083 (1993).

[8] R. Bouamrane, in *Radiative Corrections: Results and Perspectives,* edited by N. Dombey and F. Boudjema (Plenum, New York, 1990), p. 533; D. A. Dicus and W. W. Repko, Phys. Lett. B **228**, 503 (1989); Phys. Rev. D **42**, 3660 (1990); S. Dawson and G. Valencia, Nucl. Phys. **B348**, 23 (1991).

[9] J. M. Cornwall, D. N. Levin, and G. Tiktopoulos, Phys. Rev. D **10**, 1145 (1974); G. J. Gounaris, R. Kögerler, and H. Neufeld, *ibid.* **34**, 3257 (1986).

[10] M. S. Chanowitz and M. K. Gaillard, Nucl. Phys. **B261**, 379 (1985).

[11] Y.-P. Yao and C.-P. Yuan, Phys. Rev. D **38**, 2237 (1988); J.

Bagger and C. Schmidt, *ibid.* **41**, 264 (1990); H.-J. He, Y.-P. Kuang, and X. Li, Phys. Rev. Lett. **69**, 2619 (1992); Phys. Rev. D **49**, 4842 (1994).

[12] C. Grosse-Knetter, Z. Phys. C **67**, 261 (1995).

[13] A. Denner and S. Dittmaier, Phys. Rev. D **54**, 4499 (1996).

[14] M. Veltman, Acta Phys. Pol. B **8**, 475 (1977).

[15] I. Kuss and H. Spiesberger, Phys. Rev. D **53**, 6078 (1996).

[16] A. Denner, S. Dittmaier, and G. Weiglein, Nucl. Phys. **B440**, 95 (1995).

[17] A. Denner, S. Dittmaier, and R. Schuster, Nucl. Phys. **B452**, 80 (1995).

[18] A. Denner, Fortschr. Phys. **41**, 307 (1993).

[19] J. Küblbeck, M. Böhm, and A. Denner, Comput. Phys. Commun. **60**, 165 (1991); H. Eck and J. Küblbeck, Guide to FeynArts 1.0, Universität Würzburg, 1992 (unpublished); H. Eck, Dissertation, Universität Würzburg, 1995.

[20] S. Wolfram, *Mathematica—A System for Doing Mathematics by Computer* (Addison-Wesley, Redwood City, CA, 1988).

[21] G. Passarino and M. Veltman, Nucl. Phys. **B160**, 151 (1979).

[22] G. 't Hooft and M. Veltman, Nucl. Phys. **B153**, 365 (1979); A. Denner, U. Nierste, and R. Scharf, *ibid.* **B367**, 637 (1991).

[23] J. A. M. Vermaseren, *Symbolic Manipulation with FORM* (CAN, Amsterdam, 1991).

[24] R. Mertig, M. Böhm, and A. Denner, Comput. Phys. Commun. **64**, 345 (1991); R. Mertig, Guide to FeynCalc 1.0, Universität Würzburg, 1992 (unpublished).

[25] G. J. van Oldenborgh and J. A. M. Vermaseren, Z. Phys. C **46**, 425 (1990).

[26] W. Beenakker *et al.*, Phys. Lett. B **317**, 622 (1993); Nucl. Phys. **B410**, 245 (1993).

[27] L. D. Landau, Nucl. Phys. **13**, 181 (1959); R. J. Eden, P. V. Landshoff, D. I. Olive, and J. C. Polkinghorne, *The Analytic S Matrix* (Cambridge University Press, Cambridge, England, 1966).

[28] R. G. Stuart, Phys. Lett. B **262**, 113 (1991).

[29] A. Aeppli, F. Cuypers, and G. J. van Oldenborgh, Phys. Lett. B **314**, 413 (1993); A. Aeppli, G. J. van Oldenborgh, and D. Wyler, Nucl. Phys. **B428**, 126 (1994).

[30] R. G. Stuart, Report No. UM-TH-96-05, hep-ph/9603351 (unpublished).

[31] M. J. Herrero and E. Ruiz Morales, Nucl. Phys. **B437**, 319 (1995); S. Dittmaier and C. Grosse-Knetter, Phys. Rev. D **52**, 7276 (1995); Nucl. Phys. **B459**, 497 (1996).

[32] Particle Data Group, R. M. Barnett *et al.*, Phys. Rev. D **54**, 1 (1996). The most recent values can be obtained via WWW from http://pdg.lbl.gov.

[33] S. Eidelman and F. Jegerlehner, Z. Phys. C **67**, 585 (1995); H. Burkhardt and B. Pietrzyk, Phys. Lett. B **356**, 398 (1995).